Cell Reports
Medicine

Article

mRNAs encoding IL-12 and a decoy-resistant variant of IL-18 synergize to engineer T cells for efficacious intratumoral adoptive immunotherapy

Graphical abstract

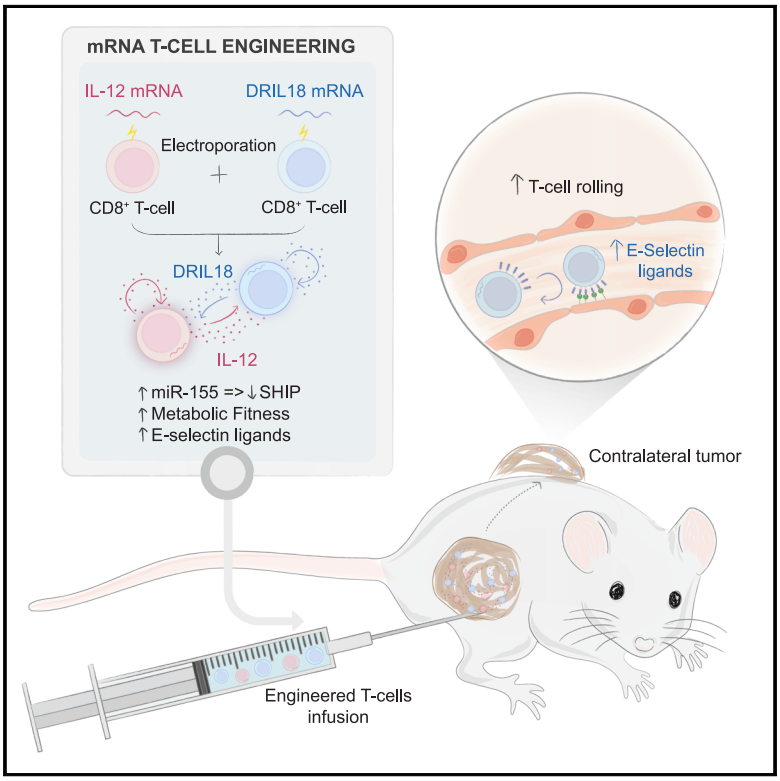

Authors

Irene Olivera, Elixabet Bolaños, Jose Gonzalez-Gomariz, ..., Gabriel A. Rabinovich, Alvaro Teijeira, Ignacio Melero

Correspondence

imelero@unav.es

In brief

Olivera et al. engineer tumor-specific T cells with mRNA to transiently express interleukin-12 (IL-12) and IL-18. Repeated intratumoral injection of IL-12/DRIL18 mRNA-electroporated T cells leads to the rejection of directly treated and distant tumors. Glycosylation changes forming E-selectin ligands, miR-155 upregulation, and improved T cell metabolic fitness underlie efficacy.

Highlights

- mRNA electroporation engineers T cells to transiently express IL-12 and DRIL18
- Intratumoral delivery of IL-12/DRIL18-engineered T cells eradicates uninjected tumors
- Enhanced efficacy depends on changes in glycosylation, miR-155, and metabolism in T cells
- Engineering TILs or CAR T cells with IL-12/DRIL18 mRNAs enhances antitumor efficacy

Olivera et al., 2023, Cell Reports Medicine *4*, 100978
March 21, 2023
https://doi.org/10.1016/j.xcrm.2023.100978

CellPress

Cell Reports Medicine

CellPress
OPEN ACCESS

Article

mRNAs encoding IL-12 and a decoy-resistant variant of IL-18 synergize to engineer T cells for efficacious intratumoral adoptive immunotherapy

Irene Olivera,[1,2,9] Elixabet Bolaños,[1,2,9] Jose Gonzalez-Gomariz,[1,2] Sandra Hervas-Stubbs,[1,2] Karina V. Mariño,[3] Carlos Luri-Rey,[1,2] Iñaki Etxeberria,[1,2] Assunta Cirella,[1,2] Josune Egea,[1,2] Javier Glez-Vaz,[1,2] Saray Garasa,[1,2,4] Maite Alvarez,[1,2,4] Iñaki Eguren-Santamaria,[1,2] Sonia Guedan,[5] Miguel F. Sanmamed,[1,2,4] Pedro Berraondo,[1,2,4] Gabriel A. Rabinovich,[6,7] Alvaro Teijeira,[1,2,10] and Ignacio Melero[1,2,4,8,10,11,*]

[1]Program of Immunology and Immunotherapy, Center for Applied Medical Research (CIMA), Pamplona, Spain
[2]Navarra Institute for Health Research (IDISNA), Pamplona, Spain
[3]Laboratorio de Glicómica Funcional y Molecular, Instituto de Biología y Medicina Experimental (IBYME), Consejo Nacional de Investigaciones Científicas y Técnicas (CONICET), Ciudad de Buenos Aires 1428, Argentina
[4]Centro de Investigación Biomédica en Red de Cáncer (CIBERONC), Madrid, Spain
[5]Department of Hematology and Oncology, Hospital Clinic, Institut d'Investigacions Biomèdiques August Pi iSunyer (IDIBAPS), Barcelona, Spain
[6]Laboratorio de Glicomedicina, Instituto de Biología y Medicina Experimental (IBYME), Consejo Nacional de Investigaciones Científicas y Técnicas (CONICET), Ciudad de Buenos Aires 1428, Argentina
[7]Facultad de Ciencias Exactas y Naturales, Universidad de Buenos Aires, Ciudad de Buenos Aires 1428, Argentina
[8]Department of Immunology and Immunotherapy, Clínica Universidad de Navarra, Pamplona, Spain
[9]These authors contributed equally
[10]Senior author
[11]Lead contact
*Correspondence: imelero@unav.es
https://doi.org/10.1016/j.xcrm.2023.100978

SUMMARY

Interleukin-12 (IL-12) gene transfer enhances the therapeutic potency of adoptive T cell therapies. We previously reported that transient engineering of tumor-specific CD8 T cells with IL-12 mRNA enhanced their systemic therapeutic efficacy when delivered intratumorally. Here, we mix T cells engineered with mRNAs to express either single-chain IL-12 (scIL-12) or an IL-18 decoy-resistant variant (DRIL18) that is not functionally hampered by IL-18 binding protein (IL-18BP). These mRNA-engineered T cell mixtures are repeatedly injected into mouse tumors. Pmel-1 T cell receptor (TCR)-transgenic T cells electroporated with scIL-12 or DRIL18 mRNAs exert powerful therapeutic effects in local and distant melanoma lesions. These effects are associated with T cell metabolic fitness, enhanced miR-155 control on immunosuppressive target genes, enhanced expression of various cytokines, and changes in the glycosylation profile of surface proteins, enabling adhesiveness to E-selectin. Efficacy of this intratumoral immunotherapeutic strategy is recapitulated in cultures of tumor-infiltrating lymphocytes (TILs) and chimeric antigen receptor (CAR) T cells on IL-12 and DRIL18 mRNA electroporation.

INTRODUCTION

Adoptive T cell therapy is achieving clinical-practice-changing success for the treatment of B cell malignances in the form of chimeric antigen receptor (CAR) T cells.[1,2] Adoptive transfer of tumor-infiltrating lymphocyte (TIL)-derived cultures is also showing efficacy against refractory cases of metastatic melanoma[3,4] and HPV$^+$ squamous carcinoma.[5] Clinical progress is also being made with T cells engineered to express tumor-specific T cell receptors (TCRs).[6–8] The field of adoptive T cell therapy offers promise to treat other malignant diseases, but results are as yet unsatisfactory against most solid tumors.

One of the main strategies to enhance the performance of adoptive T cell therapies involves the engineering of T cells, natural killer (NK) cells, or macrophages with gene-expression cassettes encoding next generation CARs, cytokines, and/or costimulatory molecules[9–12] to generate the so-called armored CARs.[13] Most popular retroviral gene-transfer strategies in lymphocytes have the inherent problem of leaving the inserted exogenous genes in the genome, resulting in long-term side effects potentially caused by the engineered cytokines.[14] Even if transcriptionally controlled systems are employed, leakiness of expression might result in serious adverse events,[14] and the co-engineering of suicide systems for safety reasons to eliminate transferred cells with drugs is problematic.[15]

mRNA engineering of T cells by electroporation is relatively simple, is clinically scalable, and can confer transient high expression of the intended exogenous proteins.[16] However, expression

extinction occurs in a few days, and hence either a reprogramming effect should last longer or repeated administrations would be needed for ultimately efficacious antitumor effects.[17]

Interleukin-12 (IL-12) is a potent immunotherapeutic cytokine in mouse models whose application as a systemic agent in the clinical setting is hampered by interferon gamma (IFN-γ)-dependent toxicity.[18] As a result, many strategies to target or express IL-12 selectively in the tumor tissue are being pursued preclinically, as well as in clinical trials.[19] Engineering T cells with IL-12 is highly efficacious in mouse models[20] but results in serious adverse events in clinical settings.[14] In contrast, IL-18 is a myeloid-derived cytokine that elicits IFN-γ expression on T and NK lymphocytes.[21] Notably, it has been reported that retrovirally transfected Pmel-1 T cells to permanently express IL-18 can promote T cell effector function and augment antitumor efficacy.[22]

IL-12 and IL-18 are known to synergize in terms of eliciting massive IFN-γ production[23] leading to severe toxic effects.[24] For cancer immunotherapy, IL-18 has the caveat of being down-regulated in its function by a decoy receptor termed IL-18 binding protein (IL-18BP),[25] which is reportedly abundant in tumor tissues.[26,27] Recently, a mutant sequence of mouse IL-18 termed DRIL18 (IL-18 decoy-resistant variant), which preserves its bioactivity but lacks binding to IL-18BP, has been reported to exert T cell-dependent antitumor activity on systemic delivery.[26] Interestingly, a similar human mutant is undergoing a phase I clinical trial (ClinicalTrials.gov: NCT04787042). In line with this, we have recently observed that mRNAs encoding single-chain IL-12 (scIL-12) and DRIL18, if expressed from the gene-transduced liver of mice, synergize to induce IFN-γ-dependent toxicity, but if delivered intratumorally, they synergize to induce antitumor effects.[24] Regarding IL-18 and adoptive T cell therapy, the group of Dr. Carl June has recently reported that anti-CD19 CAR T cells armored in the retroviral construct with a wild type IL-18 proliferate better and exert more powerful antitumor effects on intravenous delivery to mice bearing $CD19^+$ tumors.[28]

Previous work from our laboratory has shown that engineering of T cells with IL-12 and CD137L mRNAs enhanced their antitumor activity.[29] In particular, we designed a strategy based on repeated intratumoral injection into a given lesion, achieving remarkable therapeutic activity against distant non-injected tumors.[29] Notably, intratumoral delivery of immunotherapeutic agents is being extensively tested in preclinical models and in the clinic.[30] Intratumoral/local immunotherapy at present chiefly involves recombinant viruses, pathogen-associated molecular patterns and nucleic acids encoding immunostimulatory factors. Intratumoral or intracavitary use of adoptive T cell transfer[31] is also being actively used to treat primary brain tumors[32,33] and pleural malignancies[34] (ClinicalTrials.gov: NCT03054298).

In this study, we sought to improve the therapeutic strategy of intratumoral delivery of T cells transiently engineered to express IL-12. We found that IL-18 and, more prominently, DRIL18 markedly increases the efficacy of adoptive T cell immunotherapeutic strategies in a safe fashion. The mechanisms underlying this synergistic effect involved modulation of adhesion molecules, secondary cytokines, metabolic adaptations, and miR-expression regulation. Importantly, our strategy based on mRNA transient engineering and repeated intratumoral administration could be efficaciously applied when using TIL cultures or CAR T cells.

RESULTS

CD8 T cells engineered with IL-12- and DRIL18-encoding mRNAs synergize for intratumoral adoptive therapy

We previously reported the therapeutic benefit of repeated intratumoral injections of tumor-specific T cells transiently engineered with electroporated mRNA to express scIL-12.[29] To improve such a strategy, we screened the co-electroporation of several mRNAs of pro-immune genes or siRNAs for immunosuppressive genes. IL-18 mRNA was identified as a strong candidate, and a mutant sequence of mouse IL-18 has been reported to be more bioactive as it loses its repressive binding to IL-18BP,[26] which acts as a decoy receptor.

We constructed mRNAs encoding IL-18 and the IL-18 variant (DRIL18), which were electroporated into preactivated $CD8^+$Pmel-1 cells. Forty-eight-hour culture supernatants contained significant amounts of IL-18 or DRIL18 proteins produced by electroporated Pmel-1 T cells, as was also observed with scIL-12 mRNA (Figures S1A–S1C). Expression peaked at 6–12 h following electroporation, as shown in Figures S1A and S1B. Next, we co-electroporated cells with scIL-12- and DRIL18-encoding mRNAs and found that DRIL18 lowered the percentage and intensity of intracellular IL-12 expression (Figure 1A). In these experiments, we could not stain for intracellular DRIL18 because of the lack of suitable reagents. However, we found that the IL-12 released into the supernatant was not reduced if, instead of co-electroporation (IL-12 + DRIL18), single mRNA-electroporated cells were mixed 1:1 after electroporation with either scIL-12 mRNA or DRIL18 mRNA (IL-12/DRIL18), as observed on measuring IL-12 concentrations in 24-h T cell culture supernatants in these conditions (Figure 1B).

Reportedly, IL-12 and IL-18 synergize to induce IFN-γ production from T cells. In keeping with this notion, our co-electroporated (IL-12 + DRIL18) or mixed single electroporated (IL-12/DRIL18) Pmel-1 T cells released larger amounts of IFN-γ to cell culture supernatants (Figure 1C). Notably, mixed single mRNA-electroporated cells resulted in larger amounts of IFN-γ than co-electroporated cells. This was also confirmed by experiments assessing intracellular IFN-γ, whose expression was also longer in the case of the cell mixture as compared with co-electroporation (Figure 1D). More importantly, IL-18 and especially DRIL18 mRNAs enhanced the cytotoxicity of IL-12-engineered Pmel-1 T cells against ovalbumin-expressing B16 melanoma cells (B16-OVA) (Figure S1D). Cytotoxicity was greater in the case of the IL-12/DRIL18 mixtures than in the case of co-electroporated Pmel-1 lymphocytes (Figure 1E). The potentiated effect on IFN-γ production and release was found to be much higher in the case of the DRIL18 as compared with the IL-18 native sequence when combined with scIL-12. Notably, IFN-γ production seemed to last longer, at least during the first 48 h post-mRNA electroporation (Figure 1F).

We chose Pmel-1 TCR-transgenic T cells[35] because they have a low-medium avidity TCR recognizing mouse glycoprotein (gp) 100 and are known to have limited efficacy on adoptive therapeutic transfer,[36] even if electroporated to express scIL-12 mRNA.[29]

In mice bearing 8-day established subcutaneous B16-OVA melanomas in both flanks, we intratumorally injected two doses

CellPress
OPEN ACCESS

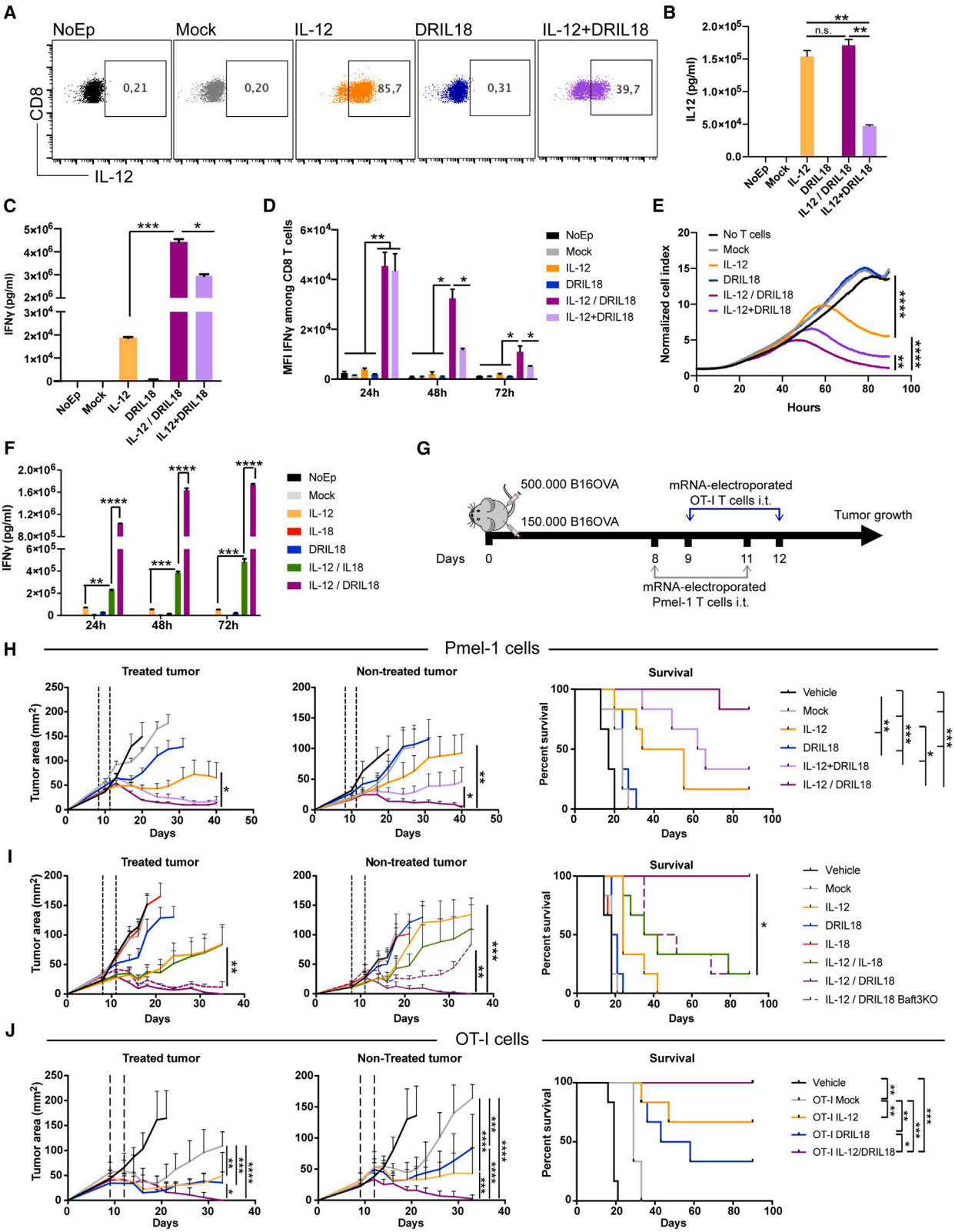

(legend on next page)

of control or mRNA-engineered Pmel-1 lymphocytes on days +8 and +11 (Figure 1G). The effect of scIL-12 and DRIL18 mRNA co-electroporation or the combination of equal quantities of both single mRNA-electroporated Pmel-1 lymphocyte cultures was tested for antitumor efficacy. Figure 1H shows that mice treated with the mixed single mRNA-electroporated Pmel-1 cells (IL-12/DRIL18) exerted better control of the injected lesion and, more importantly, eradicated the distant untreated lesions as well. Notably, unilateral intratumoral delivery attained better efficacy than intravenous delivery on both tumor lesions (Figure S2A) without any analytical or behavioral signs of toxicity (Figures S2B and S2C). In separate experiments, DRIL18 mRNA in the same setting was better than IL-18 mRNA in terms of efficacy (Figure 1I). Moreover, the distant antitumoral effect was at least partially lost in *Batf3*$^{-/-}$ mice, which specifically lack cDC1 cells,[37] indicating a need for antigen cross-presentation (Figure 1I).[38] Similar therapeutic effects were observed when mRNA-electroporated OT-I TCR transgenic lymphocytes that recognize ovalbumin residues were used in a similar bilateral B16-OVA experimental setting (Figures 1G and 1J).

Then, in order to assess the phenotype of the intratumorally adoptively transferred cells, we analyzed tumor cell suspensions of the injected and non-injected tumors as schematized in Figure S3A. In this experiment, higher percentages of IL-12/DRIL18 electroporated pmel-1 cells were found to express IFN-γ, granzyme B, Ki67, CD137, and CD25 (Figure S3B). In both the treated and non-injected tumors, there were signs of functional activation, while fewer pmel-1 cells expressed TOX as a consequence of the electroporation of the mRNAs (Figure S3B). Interestingly, when gating in endogenous CD8^{+} infiltrating tumor cells, a similar tendency to more functional activation was observed using the same markers (Figure S3C).

In mice completely rejecting their bilateral tumors following therapy with the mixtures of IL-12 and DRIL18 mRNA-engineered Pmel-1 T cells, we observed vitiligo in the area of the injected tumor (Figure S4A). Moreover, after at least 90 days, all those mice showed enhanced T cell-dependent immunity against subcutaneous rechallenges with B16-OVA, which progressed in control tumor-naive mice (Figure S4B).

The B16F10 parental cell line tends to be more refractory to immunotherapy, and treating 6-day established bilateral tumors is very challenging for any immunotherapy.[39] In the setting described in Figure S5A, increased efficacy of the mixture of DRIL18 and scIL-12 mRNA-electroporated T cells was observed, even if tumors were not completely rejected after significant, but transient, control (Figure S5A). Even when the onset of treatment was postponed until day +8, significant bilateral tumor control was achieved against the B16F10 tumors, which was found to be dependent on IFN-γ as shown by systemic *in vivo* blockade with a neutralizing monoclonal antibody (mAb) (Figure S5B).

Together, these findings highlight the greater antitumor effect of immunotherapeutic strategies involving adoptive transfer of T cells engineered to express mRNAs for IL-12 and an DRIL18.

Differential gene-expression profiles in scIL-12 versus scIL-12/DRIL18 mRNA-transduced CD8 T cells

We sought to identify the mechanisms that would account for the pronounced antitumor efficacy of the scIL-12/DRIL18 combinations. First, we performed bulk RNA sequencing (RNA-seq) analysis of antigen preactivated Pmel-1 CD8 T cell cultures transfected with scIL-12, DRIL18, or mixtures of both RNA-transduced lymphocytes in comparison with mock electroporated cells.

After 24 h of culture, principal component analyses of RNA-seq data indicated that each condition showed a unique transcriptional profile. Importantly, the mix of scIL-12 cells and DRIL18 RNA-transfected cells was particularly different in its transcriptional profile as compared with single transfected Pmel-1 lymphocytes (Figure 2A). Genes whose expression was up- or down-regulated are represented in the volcano plot shown in Figure 2B, when comparing IL-12 single-gene transfer with the one-to-one mixture of Pmel-1 cells transfected with scIL-12 or DRIL18 mRNAs. The rationale was that those genes enhanced by the combination should be important for the improvement in functional performance. Searching the lists of

Figure 1. Mixed Pmel-1 lymphocytes electroporated with scIL-12 or DRIL18 mRNA synergize for intratumoral adoptive T cell therapy

(A) Dot plots showing intensity and percentage of intracellular expression of IL-12 in preactivated Pmel-1 TCR transgenic cells with cognate peptide and electroporated 96 h later with the indicated mRNAs or a combination of scIL-12 and DRIL18 mRNAs.

(B) Corresponding concentrations of IL-12 released into the supernatant over 24 h from Pmel-1 cells either co-electroporated (IL-12 + DRIL18) or separately electroporated and subsequently mixing the cells 1:1 (IL-12/DRIL18).

(C) Concentrations of IFN-γ in the same tissue culture supernatants 72 h later.

(D) Intracellular staining to determine IFN-γ abundance by flow cytometry at the indicated time points of culture following mRNA electroporations.

(E) Performance of the electroporated Pmel-1 cells with the indicated transduced mRNAs in xCELLigence cytotoxicity assays against B16-OVA cells at an initial 1:5 ratio.

(F) Concentrations of IFN-γ over time in the different conditions of electroporated mRNA comparing electroporation with IL-12, IL-18, or DRIL18 separate single-mRNA electroporation and a subsequent mix of the cells 1:1.

(G) Experimental design of experiments treating 8-day established subcutaneous bilateral B16-OVA tumors in which only one of the tumors received electroporated Pmel-1 cells.

(H) Tumor size follow-up of injected and non-injected tumors with the indicated mock or mRNA electroporated Pmel-1 cells or vehicle. Survival of the experimental groups of mice is provided.

(I) Similar experiments as in (H) but comparing IL-18 mRNA electroporation with DRIL18 mRNA electroporation. In one condition, intratumorally treated tumor-bearing mice with IL-12/DRIL18 Pmel-1 cells were BAFT-3 knockout.

(J) Similar experiments as in (H) and (I) performed with OT-I TCR transgenic lymphocytes electroporated with the indicated mRNAs.

Experiments are representative of at least two repetitions. Biological duplicates were performed in the *in vitro* experiments (A–F). For antitumor efficacy experiments (G–J), each experimental group is composed of six mice. Data are represented as mean ± SD. Statistical comparisons were made by one-way or two-way ANOVA tests and log rank tests for Kaplan-Meier survival curves. See also Figures S1–S5 and S10.

The significance is represented with asterisks (*) according to the following values: $p<0.05$ (*), $p<0.01$(**), $p<0.001$(***) and $p<0.0001$(****).

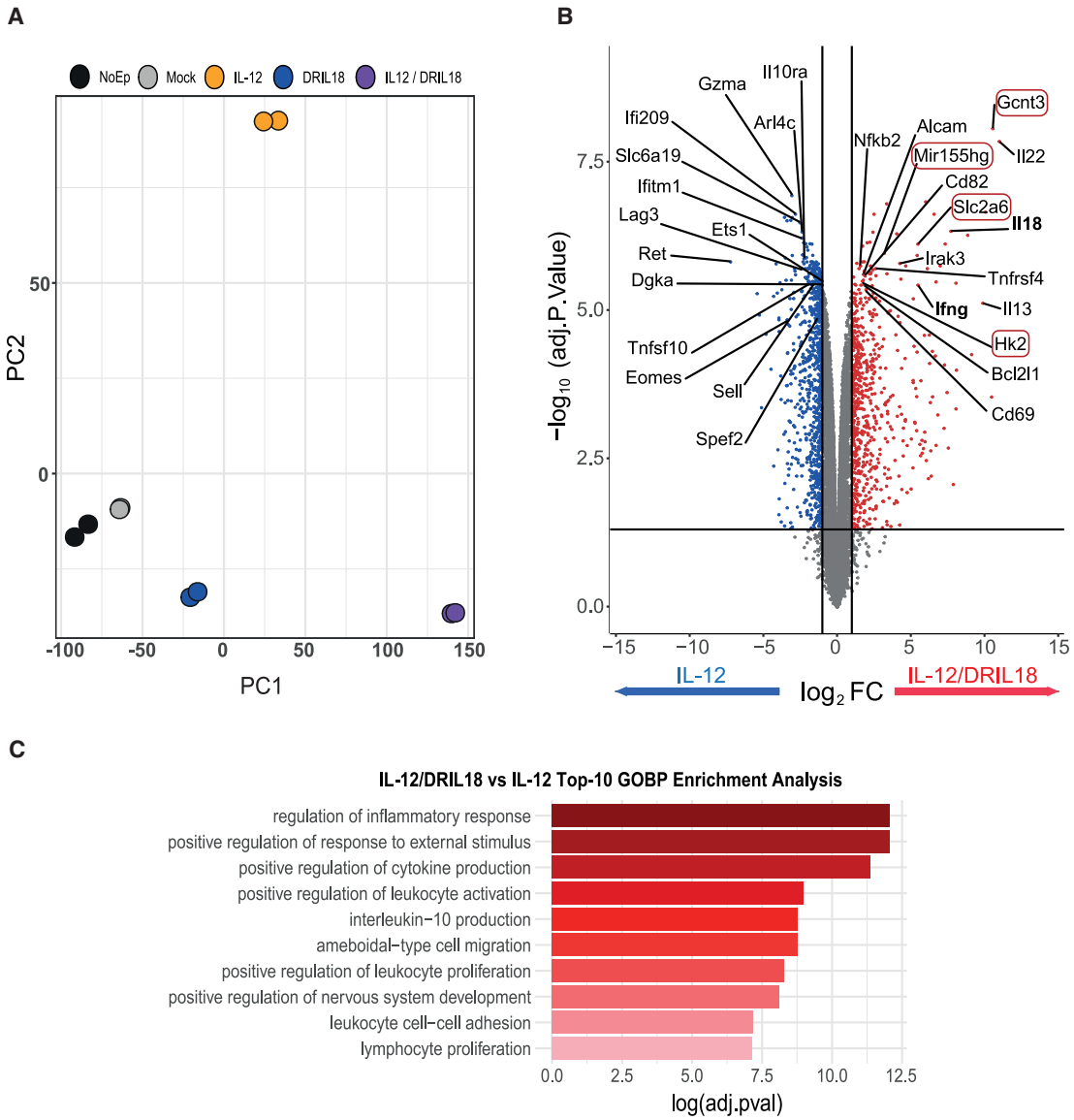

Figure 2. RNA-seq analyses of mRNA electroporated mixed Pmel-1 cells to express scIL-12 or DRIL18

(A) Principal-component analysis of the transcriptomes of 48-h antigen preactivated Pmel-1 cells transfected with the indicated mRNAs. In the case of IL-12/DRIL18, cells were separately electroporated with either single mRNA and mixed together 1:1. RNA-transduced Pmel-1 lymphocytes were cultured for an additional 24 h before retrieving the RNA.

(B) Volcano plot analysis showing genes up-regulated or down-regulated when comparing scIL-12 mRNA with the mixture of Pmel-1 cells electroporated with scIL-12 or DRIL18. Listed genes are those considered of potential functional significance for T cells, and those whose names are surrounded by red rectangles are those that we focused on in subsequent research.

(C) Top 10 biological processes obtained in Gene Ontology (GO) enrichment analysis using the up-regulated gene list of IL-12/DRIL18 vs. scIL-12 mRNA-electroporated Pmel-1 cells (adjusted P value < 0.05 and $Log_2FC > 1$) against "biological process" ontology. Experiments represent the data of two biological replicates. FC, fold change.

The significance is represented with asterisks (*) according to the following values: p<0.05 (*), p<0.01(**), p<0.001(***) and p<0.0001(****).

genes, those encoding IL-18 and IFN-γ were found, as expected. We hand-picked several other genes because of their potential function in regulating T cell-dependent responses. These genes are listed in Figure 2B, and the gene ontology functions that were found to be enriched were mostly related to T cell functionality (Figure 2C).

From the list of up-regulated genes, several caught our attention given their involvement in cytokine physiology (i.e., *Il22*), metabolic fitness (i.e., *Slc2a6*, *Hk2*), surface protein O-glycosylation (*Gcnt3*), and miR-155hg-mediated gene-expression control.[40] With regard to down-regulated genes, *Il10ra*, *Dgka*, and *Eomes* might also have a role because the first two have been involved in attenuating

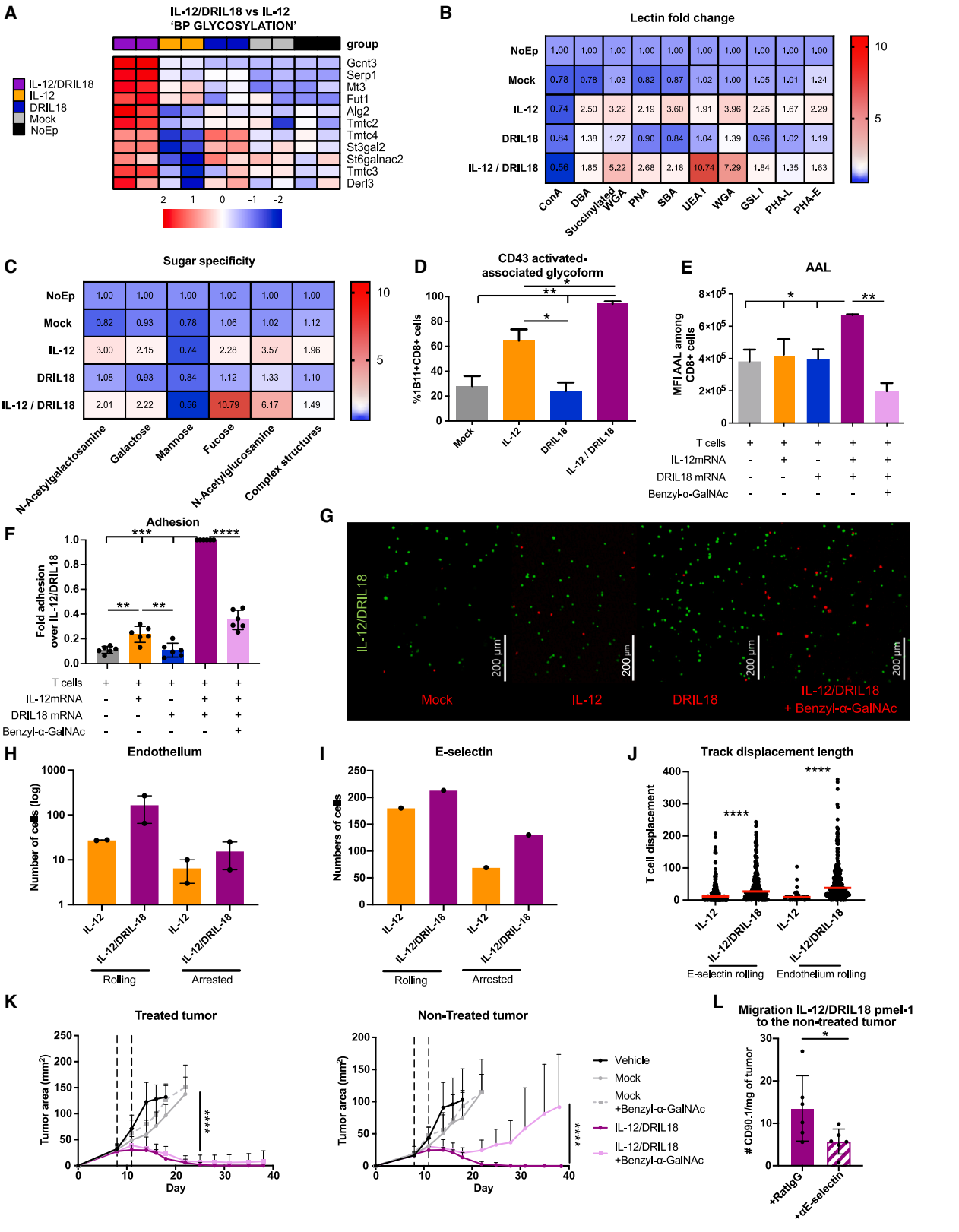

(legend on next page)

T cell activation,[41,42] and *Eomes* is implicated in the control of differentiation and effector function.[43,44]

In light of these transcriptional changes, we sought to examine the phenotypic and functional modifications underlying the potent antitumor effect generated by combined scIL-12/DRIL18 mRNAs transfection.

The scIL-12/DRIL18 mRNA combination increases E-selectin adhesion contingent on the differential glycosylation of surface proteins

Among the most prominent genes identified by the RNA-seq of the scIL-12/DRIL18 mRNA combination, our analysis revealed the up-regulated expression of *Gcnt3*-encoding mucin-type glucosaminyl (*N*-acetyl) transferase 3, a Golgi glycosyltransferase responsible for the formation of core 2 O-glycans.[45] Moreover, additional genes also involved in protein glycosylation were up-regulated (Figure 3A).

Glycophenotyping of RNA-transfected Pmel-1 T cells by flow cytometry using fluorescently labeled plant lectins (Figure 3B) showed considerable changes in the cell-surface glycosylation profile dependent on the introduction of scIL12 and DRIL18 mRNAs. Particularly, *Ulex europaeus* agglutinin I (UEA-I) and wheat germ agglutinin (WGA) binding was increased with respect to non-transfected cells, indicating that α(1,2)/α(1,3) fucosylated glycoepitopes (UEA-I) and *N*-acetylglucosamine-containing structures were increased in these cells (Figure 3C). All together, these results led us to hypothesize that scIL12 and DRIL18 mRNAs transduction increased the expression of core 2 O-glycans with terminal sialyl Lewis X (sLe^x) structures bearing (1,3) fucose.

Based on these findings, we then evaluated the expression of the activation-associated glycoform of CD43,[46] which is highly decorated with core 2 O-glycans, by flow cytometry. Using a specific antibody (1B11),[47] we observed that expression of the 1B11 epitope was increased following transfection with IL-12 mRNA and was clearly more prominent when IL-12 mRNA was combined with DRIL18 mRNA (Figure 3D). Furthermore, determination of (1,3) fucosylated glycoepitopes by flow cytometry with *Aleuria aurantia* lectin (AAL) showed a clear increase in their exposure on electroporation of the scIL-12/DRIL18 cytokine mRNAs (Figure 3E). Notably, a decrease in AAL staining was observed when we inhibited O-glycan elongation using benzyl-α-GalNAc,[48] thus substantiating the increased expression of (1,3) fucosylated O-glycans on the surface of the RNA-transferred T cells.

Given that sLe^x is a well-known ligand of E-selectin,[49] we performed competitive adhesion assays of transfected T cells to plastic-bound recombinant E-selectin. Figure 3F shows the enhanced adhesion of scIL-12/DRIL18 mRNA-transfected Pmel-1 cells to E-selectin. This effect was sensitive to inhibition by pre-exposure to Benzyl-2-acetamido-2-deoxy-α-D-galactopyranoside (benzyl-a-GalNAc), thus verifying the functional relevance of O-glycosylation in this effect. Increased competitive adhesiveness was evidenced by quantifying adhesion in microphotographs of 15-min adhesion assays (Figure 3G).

Given the reported involvement of E-selectin in leukocyte rolling,[50,51] we performed shear stress adhesion assays of fluorescently labeled lymphocytes on surface-attached tumor necrosis factor alpha (TNF-α)-activated MS1 murine microvascular endothelial cells that expressed E-selectin. Figures 3H and 3I

Figure 3. scIL-12 and DRIL18 mRNA induce changes in cell-surface glycosylation and generate E-selectin ligands important for efficacy on distant non-injected tumors

(A) Heatmap of the *Z*-scored $\log_2$counts/million (CPM) expression of differentially expressed genes with the indicated mRNAs involved in protein glycosylation showing a prominent enhancement of *Gcnt3*. "BP GLYCOSILATION" term appears as enriched in the GO analysis (adjusted P value = 0.02180856; q-value = 0.01409151).

(B) Fluorescent-lectin-binding assays represented as a matrix heatmap for binding to Pmel-1 cells transfected with the indicated mRNAs 48 h prior to the assay. Binding is represented as the fold change over non-electroporated counterparts.

(C) Grouping of the lectin-binding assays, according to their primary glycan specificity and the monosaccharide to which they bind. Complex structures indicate N-glycan-linked structures (PHA-L and PHA-E binding).

(D) Immunostaining and flow cytometry analyses of Pmel-1 cells electroporated with the indicated mRNA 48 h prior to the assay to assess the percentage of cells stained with the 1B11 mAb that detects CD43 decorated with core 2 O-glycans.

(E) Flow cytometry for quantification of α(1,3) fucosylated structures by AAL binding and evaluation of fucosylated glycoepitopes in O-glycans by inhibition with benzyl-α-GalNAc.

(F) Comparative E-selectin adhesion assays of IL-12/DRIL18-electroporated cells precultured for 48 h in comparison with the other indicated mRNAs similarly transduced cultured Pmel-1 cells. Comparative results of adhesion in 15-min assays are provided. When indicated, the O-glycosylation inhibitor benzyl-α-GalNAc was added during the 48 h preculture.

(G) Representative images of the endpoint of the adhesion assay with IL-12/DRIL18 cells are in green, while the other transduced and untransduced cells are in red.

(H) Shear stress adhesion assays under flow of the indicated mRNA-electroporated Pmel-1 cultures on MS1 mouse endothelium cells preactivated with TNF-α (see also Video S1). The number of Pmel-1 cells rolling or arrested on the endothelium are provided.

(I) Similar experiments as in (H) but performed on recombinant E-selectin attached to the bottom of the chambers.

(J) Length of the tracks of rolling Pmel-1 cells on recombinant E-selectin and endothelial cells in recorded fluorescence microscopy time-lapse videos.

(K) Treatment experiments as in Figure 1H were undertaken on B16-OVA bilateral tumor-bearing mice treated with the indicated mRNA-electroporated pmel-1 cells. In the conditions pointed out, benzyl-α-GalNAc was added during 2-h culture before *in vivo* transfer to inhibit the O-glycan elongation.

(L) Flow cytometry quantification of CD90.1$^+$ pmel-1 T cells in the contralateral tumor in experiments in which IL-12/DRIL18 mRNA-electroporated pmel-1 cells were injected into the other contralateral tumor. When indicated, mice were given neutralizing anti-E-selectin mAb.

Experiments are representative of at least two repetitions, and one-way ANOVA (D–F and L), two-way ANOVA (K), and Mann–Whitney *U* (J) tests were used for statistical comparisons. Biological duplicates were performed in experiments (A)–(H). For antitumor efficacy experiments (K and L), we randomly assigned six mice per group. Data are represented as mean ± SD. Con A, Concanavalin A; DBA, *Dolichos biflorus* lectin; GSL-I, *Griffonia simplicifolia* lectin I; PHA-E, *Phaseolus vulgaris* erythroagglutinin; PHA-L, *Phaseolus vulgaris* leucoagglutinin; PNA, peanut agglutinin; SBA, soybean agglutinin; UEA-I, *Ulex europaeus* agglutinin I; WGA, wheat germ agglutinin.

The significance is represented with asterisks (*) according to the following values: p<0.05 (*), p<0.01(**), p<0.001(***) and p<0.0001(****).

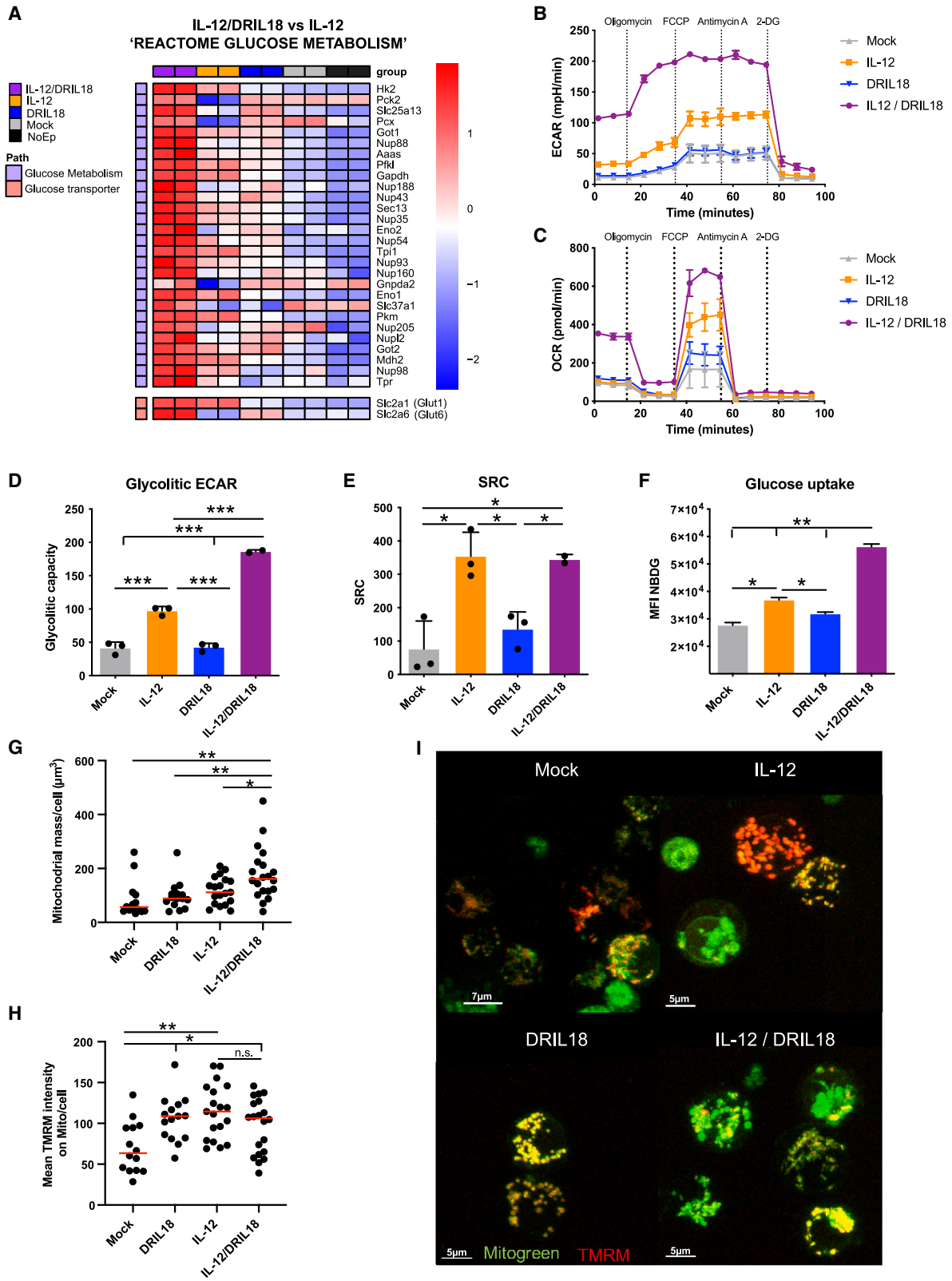

(legend on next page)

and Video S1 show that scIL-12/DRIL18 Pmel-1 cells rolled and arrested more frequently and intensely than scIL-12 single mRNA-transduced Pmel-1 T cell cultures both on microvascular endothelial cells (Figure 3H) and on plate-bound recombinant E-selectin (Figure 3I). As a consequence, the lengths of the tracks of the rolling cells were longer in such time-lapse fluorescence microscopy videos (Figure 3J). Hence the mRNA-transduced cytokines, especially IL-18, contribute to modifying adhesion of T cells to the endothelium, via modulation of their cell-surface O-glycosylation profile.

Next, we addressed whether the increased O-glycosylation could have an effect on the therapeutic efficacy. As shown in Figure 3K, preculture of the mRNA-electroporated pmel-1 cells with benzyl-α-GalNAc reduced the abscopal efficacy while preserving the effectiveness on the directly injected tumor. This could be consistent with the less efficient migration into the distant tumor. Indeed, E-selectin *in vivo* blockade with a neutralizing mAb reduced the amount of adoptively transferred mRNA-electroporated pmel-1 T cells relocated to the distant tumor (Figure 3L).

DRIL18 and scIL-12 mRNAs improve CD8 T cell metabolism involving glucose and mitochondrial fitness

In our search for additional genes that could be up-regulated by DRIL18 and scIL-12 mRNAs, we detected several genes encoding enzymes critical for glycolysis and glucose transport (Figure 4A). These include genes encoding hexokinase-2 and glut-6. In comparative Seahorse experiments assessing acidification of the medium, a stronger glycolytic rate was found that remained unaffected by drugs targeting mitochondrial functions but was drastically reduced by the glycolysis inhibitor 2-deoxyglucose (Figure 4B). Moreover, when we monitored the O_2 consumption rate, higher levels of baseline and maximal mitochondrial respiration capacity were noted in mixtures of T cells mRNA-engineered to expressed both cytokines (Figure 4C). Such results are interpreted as higher glycolysis rates (Figure 4D) and enhanced spare respiratory capacity (Figure 4E) of the mitochondria, which was mainly stimulated by the scIL-12 mRNA, while the prominent effect on glycolysis was more dependent on the IL-12/DRIL18 combination. Enhanced glucose metabolism needs more efficient glucose uptake mediated by membrane transporters, which was assessed using a fluorescent glucose probe (Figure 4F). The effect on hexokinase-II expression was confirmed by immunostaining and flow cytometry at the protein level (Figure S6A) in pmel-1 cells recovered 24 h following intratumoral delivery. In cell suspensions from individual tumors, positive correlations of average hexokinase-II expression were found with granzyme B and CD25, whereas negative correlations were observed with TOX and active caspase-3 (Figure S6B). Furthermore, we used confocal microscopy to determine variations in mitochondrial mass and transmembrane potential. Although the combination of cytokine mRNAs further enhanced mitochondrial mass (Figures 4G and 4I), transmembrane potential was similarly enhanced by either scIL-12 or DRIL18 (Figures 4H and 4I). Taken together, these results show it is likely that the enhanced glucose metabolism and mitochondrial respiration may underlie the enhanced antitumor effect of T cells driven by scIL-12 and DRIL18 mRNA.

DRIL18 and scIL-12 mRNA transfer control cytokine production and miR-155

To study whether the combination of Pmel-1 T cells transferred with mRNAs encoding scIL-12 or DRIL18 could up-regulate the cytokines implicated in the antitumor effects, we used commercial multiplex assays to analyze concentrations of several cytokines released into the culture supernatants. As shown earlier, IFN-γ was markedly increased in the 24-h supernatants of T cell mixtures transfected with the IL-12/DRIL18 mRNAs. This was also the case for interleukin-15 (IL-15), CXCL10, CCL3, and TNF-α as measured in the supernatants. Notably, type I IFNs, which are crucial for CD8 T cell responses,[52] were also up-regulated in those culture supernatants (Figure S7A).

Interestingly, the combination of scIL-12 and DRIL18 mRNAs was also able to up-regulate cytokines whose roles maybe detrimental for antitumor T cell immunity. These include the unexpected RNA-seq hit interleukin-22 (IL-22) (Figure S7B) that reportedly protects malignant epithelial cells,[53] as well as interleukin-10 (IL-10)[41] and interleukin-6 (IL-6)[54] (Figure S7B). However, IL-10 might also induce positive effects on cytotoxic lymphocyte (CTL) activation and differentiation.[55,56] In *ex vivo* cytotoxicity assays, IFN-γ blockade abrogated the cytotoxicity of the DRIL18 and scIL-12 mRNA Pmel-1 mixed cultures on

Figure 4. DRIL18 and scIL-12 mRNAs synergize to enhance glucose and mitochondrial metabolism in CD8 T cells

(A) Heatmap showing the *Z*-scored log_2CPM expression of the differentially expressed genes functionally related to glucose metabolism. The glucose metabolism pathway appears as enriched in the gene set enrichment analysis (GSEA; p-value = 0.02511886; Normalized enrichment score (NES) = 1.465072). We added two glucose transporters that were differentially expressed (Glut1 and Glut6) because of their relevance.

(B) Extracellular acidification in Seahorse assays over time of Pmel-1 cells electroporated with the indicated mRNAs 24 h prior to the assays. During the time course, the indicated compounds were added.

(C) Oxygen consumption over time of the same lymphocyte cultures.

(D) Assessment of the glycolytic rate based on acidification and the use of 2-deoxyglucose to stop glycolysis.

(E) Ratio between maximal and baseline mitochondrial respiration.

(F) Glucose intake based on internalization of the 2-(N-(7-nitrobenz-2-oxa-1,3-diazol-4-il)amino)-2-desoxiglucose (NBDG) fluorescent probe by flow cytometry and measured with arbitrary units of mean fluorescent intensity (MFI).

(G–I) Pmel-1 cells were stained with probes staining mitochondria and sensitive to mitochondrial transmembrane potential and imaged by confocal fluorescent microscopy. Quantification of mitochondrial mass per cell (G) and an estimate of transmembrane mitochondrial potential (H) are provided. Representative confocal images are shown in (I).

Experiments were repeated at least twice, and statistical comparisons were performed with one-way ANOVA tests. Biological duplicates were performed in experiments (A)–(F). Data are represented as mean ± SD. See also Figure S6.

The significance is represented with asterisks (*) according to the following values: p<0.05 (*), p<0.01(**), p<0.001(***) and p<0.0001(****).

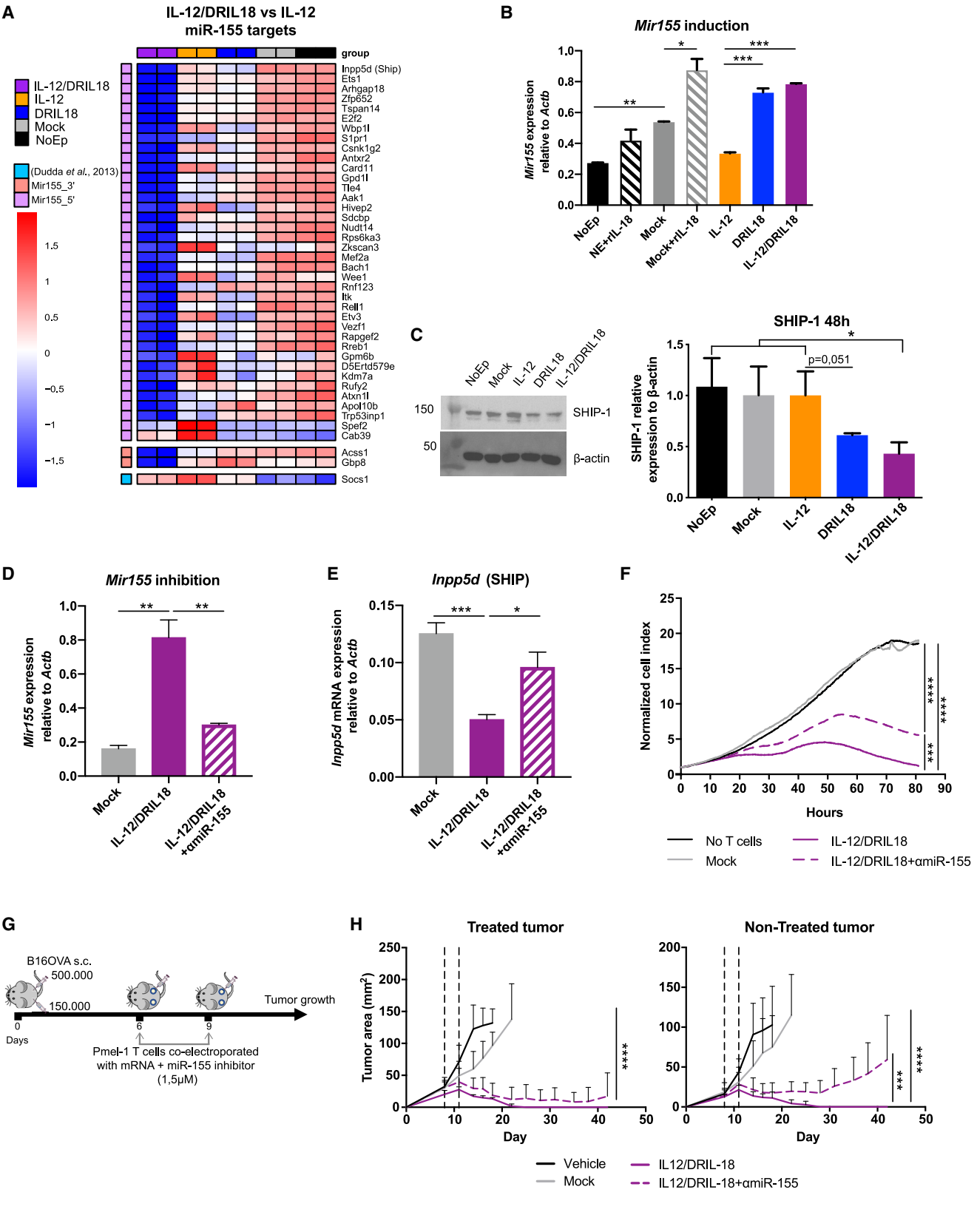

(legend on next page)

B16-OVA targets, whereas IL-22 neutralization had negligible effects (Figure S7C).

Among the genes that were substantially up-regulated in the RNA-seq studies of the scIL-12/DRIL18 combination, miR-155 emerged as an attractive mediator able to regulate multiple downstream target genes. In fact, co-cultures with scIL-12- and DRIL18-producing cells showed down-regulation of several miR-155 target genes (Figure 5A). Interestingly, increased expression of miR-155 was found to be mainly dependent on IL-18 mRNA, as shown by quantitative RT-PCR (qRT-PCR) analysis (Figure 5B).

An important miR-155 target gene controlling intracellular signaling in T cells is SHIP-1, which dephosphorylates inositol phosphates and counter-regulates phosphoinositide 3-kinase (PI3K) activity.[57,58] Western blot analysis showed down-regulation of SHIP-1 protein expression following mRNA transfer of both cytokines (Figure 5C). More abundant cytokine production and down-regulation of signal regulators of costimulatory molecules may help explain the positive combined effects of scIL-12 and DRIL18 mRNA transfer.

Next, an antagomir RNA sequence was used to reduce the expression of miR-155 on co-electroporation in IL-12/DRIL18 pmel-1 cells (Figure 5D). Such procedure also rescued the expression of *Inpp5d* (SHIP) as substantiated by qRT-PCR 24 h later (Figure 5E). Indeed, the antagomir co-electroporation also led to a decrease of secretion of IFN-γ, IL-15, IFN-α, CXCL10, and TNF-α (Figure S8A), although it did not modify the secretion of IL-6 or IL-22 (Figure S8B).

Notably, the antagomir co-electroporation attenuated the effectiveness of IL-12/DRIL18 pmel-1 lymphocytes to *ex vivo* kill B16-OVA cells in xCELLigence assays (Figure 5F) and reduced the *in vivo* therapeutic efficacy in the bilateral B16-OVA tumor model as a result of progression of the contralateral tumor lesions not directly injected with the mRNA-engineered T lymphocytes (Figures 5G and 5H).

DRIL18 and scIL-12 mRNAs synergistically enhance the performance of TILs in adoptive T cell therapy

TILs constitute a modality of adoptive T cell therapy with excellent clinical results in metastatic melanoma patients.[59] To model such activity in mice, we have reported a method to raise TIL cultures from sorted PD1$^+$CD8$^+$ TILs.[60] Before harvesting TILs, mice bearing MC38-derived tumors were treated with an anti-CD137 mAb to increase the yield of these lymphocytes. We electroporated T cell cultures either with mRNA encoding DRIL18 or scIL-12 and then used them separately or mixed. These TIL-derived cultures were used to intratumorally treat mice bearing bilateral MC38 tumors with one single dose of electroporated T cells or an equal-number mixture of lymphocytes electroporated with each cytokine mRNA (Figure 6A). Cultures were rich in lymphocytes co-expressing PD1 and CD8 (Figure 6B) and induced prominent bilateral therapeutic effects even in mice treated with only one single intratumoral dose given on day +10 after engraftment with tumor cells (Figures 6C and 6D). Such effects were considerably higher than those observed by scIL-12 mRNA single transfection (Figure 6D). Thus, scIL-12 and DRIL18 mRNA transfection act synergistically to increase the efficacy of adoptive TIL immunotherapy *in vivo*.

Greater antitumor activity of CAR T cells transduced with scIL-12 and DRIL18 mRNAs on intratumoral delivery

CAR T cells recognizing the gp75 mouse melanosomal antigen have been described.[61] The CAR construct carries an EGFP reporter gene to monitor the gene transfer of splenocytes that were preactivated with anti-CD3 and anti-CD28 mAbs. CAR gene transfer attained over 90% transduction efficiency using a retroviral vector (Figure S9A). Such cultures could be electroporated with mRNAs undergoing only a moderate loss of their viability (Figure S9B). These mRNA-electroporated T cells were able to express scIL-12, which was detected intracellularly at the protein level (Figure 7A). In these CAR T cell cultures, scIL-12 and DRIL18 mRNAs also synergized to induce the secretion of high amounts of IFN-γ into the culture supernatants (Figure 7B). Moreover, the combination of IL-12 and DRIL18 mRNA-modified CARs synergized in *ex vivo* toxicity assays to kill B16-OVA target cells stably transfected to overexpress gp75 (Figure 7C) or even untransfected B16-OVA melanoma cells (Figure 7D).

Using these mRNA-transduced CAR T cell cultures, we set up experiments to treat bilaterally B16-OVA-bearing mice in which

Figure 5. Mixed scIL-12/DRIL18 electroporated Pmel-1 cells upregulate functional miR-155 that is involved in the therapeutic efficacy

(A) Heatmap showing down-regulation of the *Z* score $\log_2$CPM of differentially expressed genes reported as miR-155 target genes in the mixes of scIL-12/DRIL18 Pmel-1 cells. GSEA shows enrichment in miR-155-5′ targets gene set (p.val = 0.0009229154; NES = −1.654717). We added more differentially expressed (DE) genes genes that are targets of miR-155-3′ (Acss1 and Gbp8) and Socs1, a well-known target of miR-155-5′ not described in the M3 category.

(B) Confirmation of the up-regulation of *Mir155* by quantitative RT-PCR (qRT-PCR).

(C) Immunoblot analysis of SHIP-1 expression in the indicated Pmel-1 mRNA-transfected cells as compared with β-actin. Relative densitometry data are shown in the bar graph.

(D) An antagomir RNA was co-electroporated to induce the degradation of miR-155 (αmiR-155) as compared with the negative control antagomir co-electroporated with IL-12/DRIL18 mRNAs.

(E) The antagomir partially rescued the mRNA expression of *Inpp5d* (SHIP) in the IL-12/DRIL18 pmel-1 cells as assessed by qRT-PCR.

(F) IL-12/DRIL18 pmel-1 cells co-electroporated with the antagomir degrading miR-155 exhibited less efficacious *ex vivo* cytotoxicity against B16-OVA as assessed by xCELLigence assays.

(G and H) Efficacy experiments in mice bearing bilateral B16-OVA tumors that show that co-electroporation of the antagomir (αmiR-155) reduced the bilateral efficacy of IL-12/DRIL18 electroporated pmel-1 cells injected to one of the tumors. Statistical comparisons were performed using one-way ANOVA (B–E) or two-way ANOVA tests (H). Experiments were repeated at least twice.

Biological duplicates were performed in experiments (A)–(F). For antitumor efficacy experiments (G and H), we randomly assigned six mice per group. Data are represented as mean ± SD. See also Figures S7 and S8.

The significance is represented with asterisks (*) according to the following values: p<0.05 (*), p<0.01(**), p<0.001(***) and p<0.0001(****).

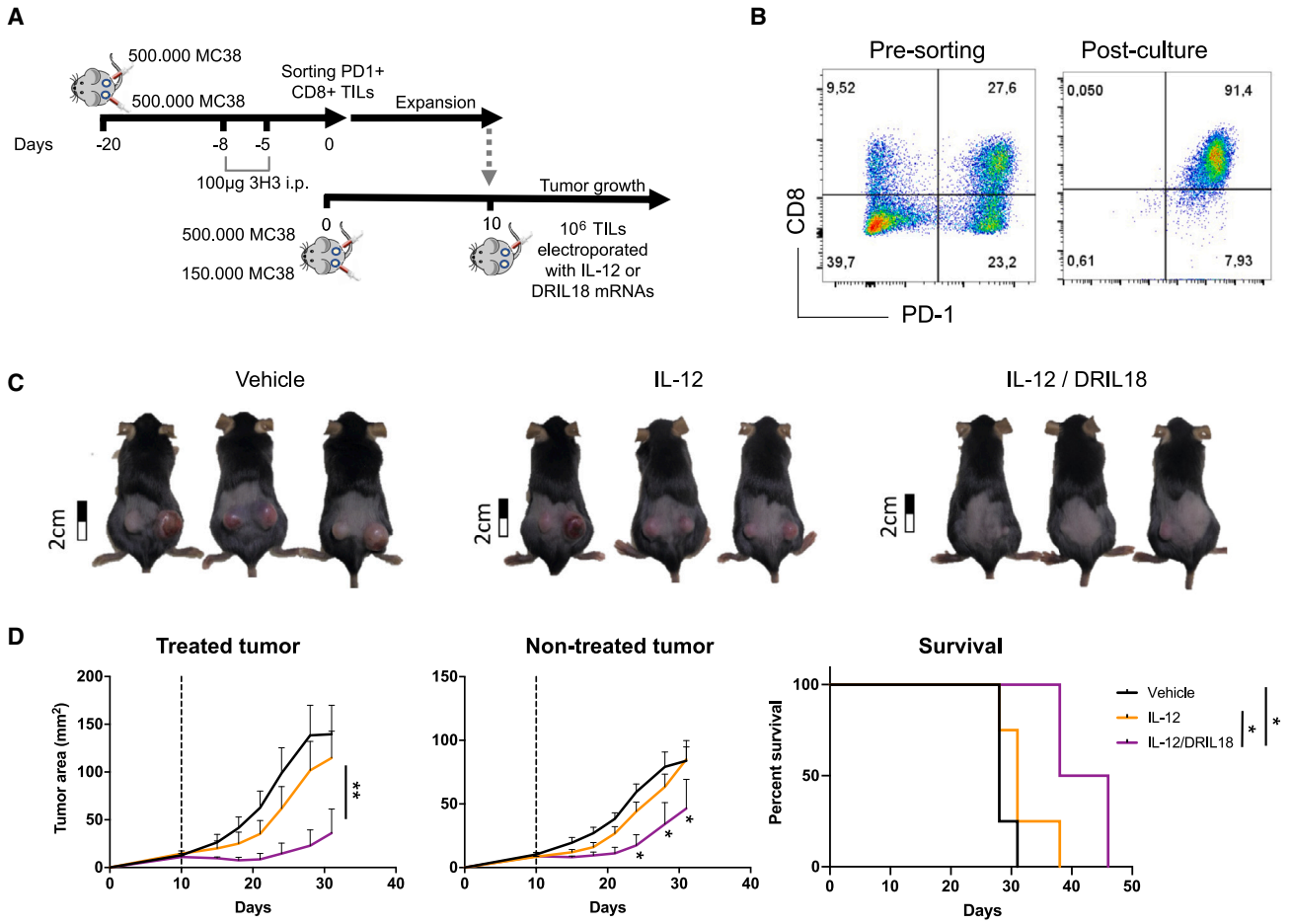

Figure 6. Mixing tumor-infiltrating lymphocyte (TIL) cultures electroporated with scIL-12 mRNA and DRIL18 mRNA synergize for intratumoral adoptive T cell therapy

(A) Scheme of generation of TIL cultures from MC38 tumors and treatment of mice bearing bilateral MC38 tumors following mRNA electroporation.

(B) Dot plot graphs of cell suspensions derived from tumors and TILs post-culture stained with anti-PD1 and anti-CD8 mAbs.

(C) Representative photographs of treated mice with the indicated mRNA-transfected TILs on day +30.

(D) Tumor size follow-up and survival of the indicated groups of mice.

Log rank tests were used to compare survival curves, and two-way ANOVA tests were used to compare tumor growth. Experiments were repeated three times, and we randomly assigned six mice per group. Data are represented as mean ± SD.

The significance is represented with asterisks (*) according to the following values: $p<0.05$ (*), $p<0.01$(**), $p<0.001$(***) and $p<0.0001$(****).

only one of the tumors was intratumorally treated on days +8 and +11 (Figure 7E). The mixtures of CAR T cells transfected with either cytokine mRNA showed a synergistic antitumor effect against directly injected and non-injected contralateral tumors (Figure 7F).

Collectively, these data highlight the therapeutic value of mRNA transient cytokine gene transfer, especially in those approaches showing synergistic effects to enhance the functional performance of CAR T cells, at least for local delivery strategies.

DISCUSSION

In previous work, we showed the efficacy of using scIL-12 mRNA-transfected TCR-transgenic CD8 T cells for repeated intratumoral delivery.[29] Such efficacy was extended to mouse and human TILs.[29] The repeated intralesional strategy is considered feasible in the clinic;[62] hence we sought to improve its efficacy with the addition of other transgenes. Our screenings led to the identification of IL-18[63] as a suitable synergistic partner for the IL-12 mRNA transgene.

Studies of these synergistic effects using IL-18- and scIL-12-encoding mRNAs revealed that mixing single mRNA-transfected T cells with either DRIL18 or scIL-12 by electroporation was more efficacious than co-electroporating both mRNAs in the same cells. The reason seems to be related to a competitive reduction of mRNA expression of the two optimized mRNAs in the same cell because of as yet poorly understood reasons. The mixtures of T cells with different electroporated mRNAs seem to be advantageous in this system and would permit fine-tuning of the proportions of mixed cells to optimize efficacy and safety.

Using Pmel-1 anti-gp100 and anti-OVA OT-I TCR-transgenic cells[35] transduced with DRIL18 and scIL-12 mRNAs, we

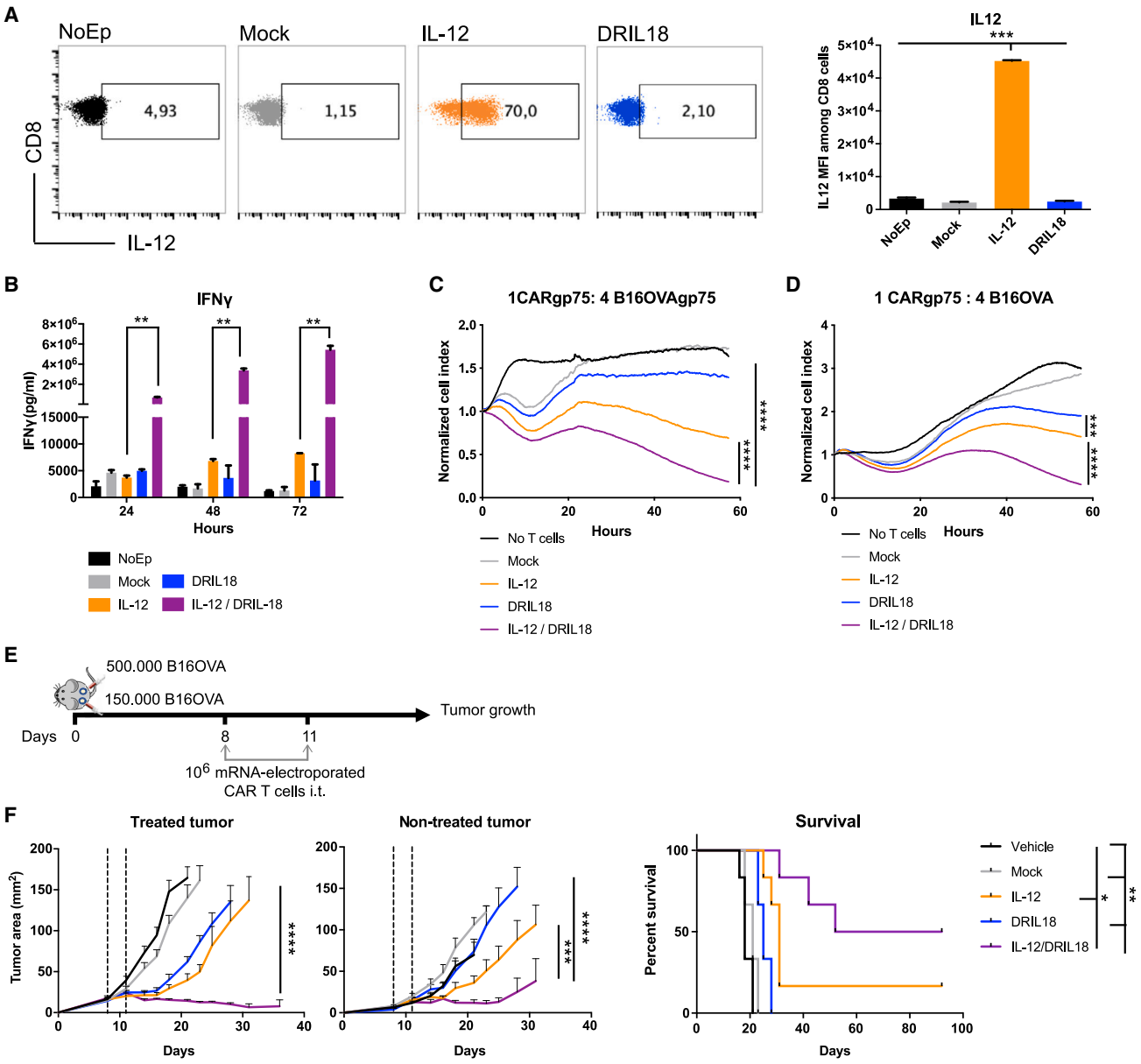

Figure 7. Improved therapeutic efficacy of intratumoral injections with gp75-recognizing CAR T cells following scIL-12/DRIL18 mRNA electroporation

(A) Intracellular IL-12 protein expression following electroporation of the indicated mRNAs into anti-gp75 mouse CAR T cells. MFIs are provided in the bar graph.

(B) IFN-γ concentrations over time in the indicated CAR T cell cultures, including the mixes of DRIL18 and scIL-12 CAR T cells.

(C and D) *Ex vivo* cytotoxicity performed over time with the indicated mRNA-electroporated CAR T cells at a 1:4 ratio against gp75-transfected B16-OVA (C) and non-transfected B16-OVA (D).

(E) Scheme of the experiments of mice bearing bilaterally B16-OVA tumors and treated intratumorally with the different mRNA-electroporated CAR T cells or the scIL-12/DRIL18 mixture.

(F) Tumor size follow-up of CAR T-injected and contralateral non-injected tumors with the indicated mRNA-electroporated or mock CAR T cells. Survival of the treatment groups of mice is provided.

Experiments were repeated twice, and statistical comparisons were made with one-way ANOVA tests (A and B), two-way ANOVA tests, and log rank tests to compare tumor growth and survival, respectively. Biological duplicates were performed in experiments (B)–(D). For antitumor efficacy experiments (E and F), we randomly assigned six mice per group. Data are represented as mean ± SD. See also Figure S9.

The significance is represented with asterisks (*) according to the following values: $p<0.05$ (*), $p<0.01$(**), $p<0.001$(***) and $p<0.0001$(****).

observed unprecedented efficacy not only against the treated tumor but also against distant well-established tumor lesions. The main rationale for using an intratumoral delivery route is to provide immediate antigen contact of all the injected T lymphocytes at the time point when the mRNA-encoded transgenes are most prominently expressed. Killing a fraction of tumor cells in an immunogenic fashion to create an *in situ* vaccine is also desirable.[64,65] Thus, the strategy may be potentiating cross-priming and epitope antigen spreading[66] as we have previously shown.[29] The importance of recruiting a polyclonal endogenous T cell response is paramount, for instance, to avoid escape of antigen-loss variants. Of important note, IL-12/DRIL18 direct intratumoral delivery of the naked mRNA as recently reported[24] was less effective than intratumoral delivery of the electroporated tumor-specific CD8 T cells with the same mRNAs (Figure S10).

From the injection site, T cells would need to reach the circulation in order to gain access to distant metastatic sites. In the case of clinical application, intratumoral delivery and systemic infusion could be combined. Local delivery of adoptive T cell transfer is gaining clinical momentum for brain tumors[32,33] and intracavitary malignances[34] (ClinicalTrials.gov: NCT03054258) and has shown reasonable safety and efficacy in a number of clinical trials.[31] For clinical translation of the intratumoral route, image-guided injection[62] or the use of implanted surgical catheters[32,33] are feasible options.

One key question was to elucidate the mechanisms underlying the observed remarkable synergy. Notably, we used a mutant form of IL-18 that is not repressible by IL-18BP, thereby bypassing this regulatory barrier to achieve maximal effects.[24,26] Indeed, large amounts of IFN-γ were secreted by the mRNA-engineered T cells, and IFN-γ was shown to be essential to attain maximal therapeutic efficacy. Using RNA-seq experiments, we found a number of DRIL18-regulated transcripts potentially underpinning the enhanced functional performance of the engineered CD8 T cells. We interrogated differential glycosylation of cell-surface proteins following discovery of a prominent up-regulation of the Gcnt3 glycosyltransferase. We found considerable remodeling of glycosylation, which enabled expression of E-selectin ligands on the surface of T cells. Given the broad impact of glycosylation on T cell function, including cell adhesion and trafficking,[67,68] we examined the biological relevance of scIL-12/DRIL18-driven glycan changes in T cell adhesion assays. Interestingly, changes in the O-glycosylation profile resulted in enhanced adhesion of T cells to microvascular endothelial cells. Moreover, inhibition of O-glycan elongation with benzyl-α-GalNac resulted in less efficacy on *in vivo* intratumoral treatments observed in the non-injected tumors. This seems to be associated with less efficient migration to the contralateral tumor lesions, as shown on mAb-mediated E-selectin blockade.

In search of the additional mechanisms underlying the potent antitumoral effects of DRIL18- and scIL-12-engineered Pmel-1, we also explored their hierarchical modulation of secondary cytokines. In fact, several cytokines were found to be up-regulated when DRIL18 and scIL-12 acted in concert. These include IL-15 and type I IFNs, both known to regulate the function and survival of cytotoxic T lymphocytes.[69,70] These and other induced cytokines probably contribute in a paracrine or autocrine fashion for the overall antitumor efficacy. Notably, up-regulation of miR-155 by scIL-12 and DRIL18 mRNAs successfully reduced SHIP-1 and SOCS-1 expression, potentially enhancing responsiveness to costimulatory molecules engaging PI3K,[58] as well as responsiveness to homeostatic and inflammatory cytokines.[57,71,72] Indeed, the expression of miR155hg is reportedly associated with better survival in several malignancies and with signs of more prominent infiltration by immune cells.[40] Co-electroporation of an antagomir inducing the degradation of miR-155 established the role of miR-155 in the contralateral antitumor effect associated with increased *ex vivo* cytotoxicity and cytokine production. The connection of miR-155 induction and IL-12/DRIL18 stimulation in terms of mechanism remains elusive but might offer other opportunities for intervention.

Interestingly, we also found that DRIL18 and scIL-12 mRNAs induced changes in the glucose metabolism of T cells, including enhanced glycolysis and mitochondrial function. Indeed, T cell metabolic fitness is considered key for the success of adoptive T cell therapy and the antitumor performance of T cells,[73–75] especially in the case of hypoxic solid tumors.[76] Therefore, we found that IL-18 enhances CTL responses, and that the DRIL18 variant excels at performing such a function.

When envisioning the behavior of mixed T cell populations injected intratumorally, it is expected that they will produce high quantities of the synthetic mRNA-encoded cytokines. Such cytokines would exert autocrine and paracrine effects on injected T cells and presumably also on endogenous T and NK cells, which also express receptors for IL-12 and IL-18. In this context, cytotoxic tumor cell death will take place fostering inflammation and making tumor antigens available for cross-presentation.[77] Notably, cDC1-deficient BATF-3 knockout (KO) mice are resistant to the systemic effects of this immunotherapy strategy. The artificial production of IL-12 by the Pmel-1 cells probably bypasses one of the key functions of cDC1, which is IL-12 production, but not cross-presentation itself.[78] In addition, high local amounts of IFN-γ are expected to acutely exert antitumor effects[79] and foster antigen presentation[80] but might also turn on immunosuppressive feedback mechanisms such as Programmed death-ligand 1 (PD-L1) and Idoleamine 2,3-dioxygenase 1 (IDO-1) expression.[81]

In our previous report with scIL-12 mRNA, we described active T cell trafficking from the injected to the non-injected tumor sites. The induction of E-selectin ligands by the combination of scIL-12/DRIL18 mRNAs should help mediate these processes, at least facilitating rolling and arrest on tumor endothelial cells for extravasation in a concerted function with leukocyte integrins.[82] Indeed, changes in O-glycosylation profiles were found to be underpinning the bilateral tumor efficacy.

Our proof-of-concept experiments with TILs and CAR T cells showed remarkable efficacy on single-mRNA electroporation of scIL-12 and DRIL18 and mixing such lymphocyte cultures for subsequent intratumoral delivery. These approaches are clinically feasible. Our current IND-oriented research involves mainly the electroporation of TILs for repeated intratumoral and systemic delivery using frozen batches of the cell therapy products. The strategy can also work with CAR T cells recognizing tumor antigens in solid tumors. The transient expression of the transgenes in the form of mRNAs was well tolerated in mice, and

intratumoral release represents an excellent choice to mitigate systemic cytokine-mediated side effects. Repeated injection would be feasible using frozen aliquots, and intratumoral delivery is also feasible and likely to reduce the number of cells in the required lymphocyte doses. In the case of CAR T immunotherapy, repeated local treatment of peritoneal carcinomatosis in ovarian cancer patients with anti-mesothelin CAR T cells makes sense,[83] and using the intratumoral route with anti-mesothelin CAR T cells has been already clinically pioneered by the group of Michael Sadelain[34] in the case of malignant mesothelioma. Notably, IL-12 mRNA-engineered OT-I cells have been recently reported to be efficacious for models of peritoneal carcinomatosis when they are intraperitoneally delivered.[84] Repeated local treatments with these CAR T cells engineered with cytokine-encoding mRNAs make special sense.

In conclusion, we report on a substantial improvement of an adoptive T cell therapy strategy based on mRNA transient gene transfer and repeated intratumoral delivery. The synergistic immunobiology of IL-12 and IL-18, best represented in the form of DRIL18, holds promise for efficacious outcomes in the treatment of metastatic cancer patients.

Limitations of the study

In spite of the fact that experimental antitumor efficacy has been demonstrated with TILs, CAR T cells, and TCR-transgenic mouse T cells, it is essential to confirm our results in other experimental models of adoptive T cell therapy. The mouse immune system is similar to a certain degree to the human one. However, the results obtained in mice frequently do not reproduce the clinical reality.

Furthermore, our mRNA electroporation strategy has a limitation, which is the inability to productively electroporate multiple mRNAs to the same T cell. The expression of each protein decreased when we tried to co-electroporate. Improvements in the mRNA design or in the electroporation techniques could optimize such results toward clinical development.

Glycosylation changes generating E-selectin ligands, miR155, cytokines, and metabolic improvements are clearly involved mechanisms underlying efficacy, but other yet to be identified factors may contribute.

STAR★METHODS

Detailed methods are provided in the online version of this paper and include the following:

- KEY RESOURCES TABLE
- RESOURCE AVAILABILITY
  - Lead contact
  - Materials availability
  - Data and code availability
- EXPERIMENTAL MODEL AND SUBJECT DETAILS
  - Mice
  - Tumor cell lines
  - Primary cells
- METHOD DETAILS
  - Vector constructs, mRNA *in vitro* transcription and mRNA transduction by electroporation
  - Mouse lymphocyte isolation, activation and expansion
  - Retroviral transduction of mouse T cells
  - Mouse TIL isolation, sorting and expansion
  - *In vivo* tumor inoculation, adoptive T cell transfer and treatments
  - *In vivo* neutralization and inhibition experiments
  - Adoptively transfer and endogenous T cell characterization
  - Flow cytometry
  - Serum toxicity determination
  - *In vitro* cytotoxicity assays (xCELLigence)
  - Adhesion assays
  - Flow adhesion assays
  - Mitochondria staining
  - Cytokine measurement in T-cell culture supernatants
  - Seahorse and glucose uptake assays
  - Western blots
  - RNA extraction and quantitative RT-PCR
  - RNAseq sample preparation and bioinformatic analysis
- QUANTIFICATION AND STATISTICAL ANALYSES

SUPPLEMENTAL INFORMATION

Supplemental information can be found online at https://doi.org/10.1016/j.xcrm.2023.100978.

ACKNOWLEDGMENTS

We are grateful to Dr. Ana Rouzaut and María C. Ochoa for helpful scientific discussions. We also acknowledge Diego Alignani from the flow cytometry facilities and Eneko Elizalde, Alberto Espinal, and Elena Ciordia from the animal facility for their excellent work. This project has been supported by MINECO PID2020-112892RB-100 and PID2020-113174-RA-100 (MCIN/AEI/10.13039/501100011033, AEI/FEDER, UE), supported by Instituto de Salud Carlos III (PI19/01128), and cofinanced by Fondos FEDER "A way to make Europe," by the I-ON network supported by Bristol Myers Squibb (to I.M.). This project has received funding from the European Union's Horizon 2020 research and innovation program (grant 945393- T2EVOLVE and Marie-Sklodowska-Curie grant 765394), Fundación de la Asociación Española Contra el Cáncer (AECC) GCB15152947MELE, Fundació la Marató de TV3 (488/C/2019), Fundación La Caixa HR21-00083 and Fundación BBVA, Gobierno de Navarra Salud GN 39–2021, Gobierno de Navarra Proyecto LINTERNA ref. 0011–1411-2020-000075, Mark Foundation, and Fundación Olga Torres. A.T. was supported by the Ramon y Cajal program from the Spanish Ministry of Science (RyC 2019-026406-I). I.O. received a scholarship from FPI program PRE2018-085962 (MINECO). S.H.-S. was supported by "Fundación AECC" (IDEAS18121HERV). M.A. was supported by the Spanish Association Against Cancer's Investigator grant (INVES19041ALVA). Work in G.A.R.'s lab was supported by a grant from Agencia Nacional de Promoción de la Investigación, el Desarrollo Tecnológico y la Innovación (PICT 2020-1552).

AUTHOR CONTRIBUTIONS

Conceptualization, I.O., E.B., A.T., and I.M.; methodology, I.O., E.B., S.H.-S., J.E., S.G., M.A., K.V.M., A.T., and I.M.; formal analysis, I.O., E.B., J.G.-G., and A.T.; investigation, I.O., E.B., G.A.R., S.G., M.A., J.G.-V., C.L.-R., A.C., I.E., I.E.-S., M.F.S., P.B., A.T., and I.M.; resources, S.H.-S. and S.G.; writing – original draft, I.O., A.T., and I.M.; writing – review & editing, all authors; visualization, I.O., J.G.-G., C.L.-R., and A.T.; supervision, I.M. and A.T.; project administration, I.O., E.B., A.T., and I.M.; funding acquisition, A.T., M.A., S.H.-S., and I.M.

DECLARATION OF INTERESTS

I.M. acknowledges grants from Roche, Alligator, Genmab, BMS, AstraZeneca, Pharmamar, and Bioncotech, as well as consultancy fees from BMS, Roche, Genmab, Numab, Pieris, Catalym, F-STAR, Third Rock, Amunix, Gossamer, Alligator, AstraZeneca, and Pharmamar. M.F.S. has received a grant from Roche.

INCLUSION AND DIVERSITY

We support inclusive, diverse, and equitable conduct of research.

Received: July 28, 2022
Revised: December 22, 2022
Accepted: February 21, 2023
Published: March 14, 2023

REFERENCES

1. June, C.H., O'Connor, R.S., Kawalekar, O.U., Ghassemi, S., Milone, M.C., O'Connor, R.S., Kawalekar, O.U., Ghassemi, S., and Milone, M.C. (2018). CAR T cell immunotherapy for human cancer. Science *359*, 1361–1365. https://doi.org/10.1126/science.aar6711.
2. Young, R.M., Engel, N.W., Uslu, U., Wellhausen, N., and June, C.H. (2022). Next-Generation CAR T-Cell Therapies (Cancer Discov), CD-21-1683. https://doi.org/10.1158/2159-8290.
3. Rosenberg, S.A., Yang, J.C., Sherry, R.M., Kammula, U.S., Hughes, M.S., Phan, G.Q., Citrin, D.E., Restifo, N.P., Robbins, P.F., Wunderlich, J.R., et al. (2011). Durable complete responses in heavily pretreated patients with metastatic melanoma using T-cell transfer immunotherapy. Clin. Cancer Res. *17*, 4550–4557. https://doi.org/10.1158/1078-0432.CCR-11-0116.
4. Dudley, M.E., Gross, C.A., Somerville, R.P.T., Hong, Y., Schaub, N.P., Rosati, S.F., White, D.E., Nathan, D., Restifo, N.P., Steinberg, S.M., et al. (2013). Randomized selection design trial evaluating CD8 + -enriched versus unselected tumor-infiltrating lymphocytes for adoptive cell therapy for patients with melanoma. J. Clin. Oncol. *31*, 2152–2159. https://doi.org/10.1200/JCO.2012.46.6441.
5. Stevanović, S., Helman, S.R., Wunderlich, J.R., Langhan, M.M., Doran, S.L., Kwong, M.L.M., Somerville, R.P.T., Klebanoff, C.A., Kammula, U.S., Sherry, R.M., et al. (2019). A phase II study of tumor-infiltrating lymphocyte therapy for human papillomavirus–associated epithelial cancers. Clin. Cancer Res. *25*, 1486–1493. https://doi.org/10.1158/1078-0432.CCR-18-2722.
6. Robbins, P.F., Kassim, S.H., Tran, T.L.N., Crystal, J.S., Morgan, R.A., Feldman, S.A., Yang, J.C., Dudley, M.E., Wunderlich, J.R., Sherry, R.M., et al. (2015). A pilot trial using lymphocytes genetically engineered with an NY-ESO-1–Reactive T-cell receptor: long-term follow-up and correlates with response. Clin. Cancer Res. *21*, 1019–1027. https://doi.org/10.1158/1078-0432.CCR-14-2708.
7. Doran, S.L., Stevanović, S., Adhikary, S., Gartner, J.J., Jia, L., Kwong, M.L.M., Faquin, W.C., Hewitt, S.M., Sherry, R.M., Yang, J.C., et al. (2019). T-cell receptor gene therapy for human papillomavirus–associated epithelial cancers: a first-in-human, phase I/II study. J. Clin. Oncol. *37*, 2759–2768. https://doi.org/10.1200/JCO.18.02424.
8. Rapoport, A.P., Stadtmauer, E.A., Binder-Scholl, G.K., Goloubeva, O., Vogl, D.T., Lacey, S.F., Badros, A.Z., Garfall, A., Weiss, B., Finklestein, J., et al. (2015). NY-ESO-1-specific TCR-engineered T cells mediate sustained antigen-specific antitumor effects in myeloma. Nat. Med. *21*, 914–921. https://doi.org/10.1038/NM.3910.
9. Abdin, S.M., Paasch, D., Morgan, M., and Lachmann, N. (2021). CARs and beyond: tailoring macrophage-based cell therapeutics to combat solid malignancies. J. Immunother. Cancer *9*, e002741. https://doi.org/10.1136/jitc-2021-002741.
10. Stephan, M.T., Ponomarev, V., Brentjens, R.J., Chang, A.H., Dobrenkov, K.V., Heller, G., and Sadelain, M. (2007). T cell–encoded CD80 and 4-1BBL induce auto- and transcostimulation, resulting in potent tumor rejection. Nat. Med. *13*, 1440–1449. https://doi.org/10.1038/nm1676.
11. Daher, M., Basar, R., Gokdemir, E., Baran, N., Uprety, N., Nunez Cortes, A.K., Mendt, M., Kerbauy, L.N., Banerjee, P.P., Shanley, M., et al. (2021). Targeting a cytokine checkpoint enhances the fitness of armored cord blood CAR-NK cells. Blood *137*, 624–636. https://doi.org/10.1182/blood.2020007748.
12. Yeku, O.O., Purdon, T.J., Koneru, M., Spriggs, D., and Brentjens, R.J. (2017). Armored CAR T cells enhance antitumor efficacy and overcome the tumor microenvironment. Sci. Rep. *7*, 10541. https://doi.org/10.1038/s41598-017-10940-8.
13. Yeku, O.O., and Brentjens, R.J. (2016). Armored CAR T-cells: utilizing cytokines and pro-inflammatory ligands to enhance CAR T-cell anti-tumour efficacy. Biochem. Soc. Trans. *44*, 412–418. https://doi.org/10.1042/BST20150291.
14. Zhang, L., Morgan, R.A., Beane, J.D., Zheng, Z., Dudley, M.E., Kassim, S.H., Nahvi, A.V., Ngo, L.T., Sherry, R.M., Phan, G.Q., et al. (2015). Tumor-infiltrating lymphocytes genetically engineered with an inducible gene encoding interleukin-12 for the immunotherapy of metastatic melanoma. Clin. Cancer Res. *21*, 2278–2288. https://doi.org/10.1158/1078-0432.CCR-14-2085.
15. Bonini, C., and Mondino, A. (2015). Adoptive T-cell therapy for cancer: the era of engineered T cells. Eur. J. Immunol. *45*, 2457–2469. https://doi.org/10.1002/eji.201545552.
16. Zhao, Y., Moon, E., Carpenito, C., Paulos, C.M., Liu, X., Brennan, A.L., Chew, A., Carroll, R.G., Scholler, J., Levine, B.L., et al. (2010). Multiple injections of electroporated autologous T cells expressing a chimeric antigen receptor mediate regression of human disseminated tumor. Cancer Res. *70*, 9053–9061. https://doi.org/10.1158/0008-5472.CAN-10-2880.
17. Etxeberria, I., Olivera, I., Bolaños, E., Cirella, A., Teijeira, Á., Berraondo, P., and Melero, I. (2020). Engineering bionic T cells: signal 1, signal 2, signal 3, reprogramming and the removal of inhibitory mechanisms. Cell. Mol. Immunol. *17*, 576–586. https://doi.org/10.1038/s41423-020-0464-1.
18. Del Vecchio, M., Bajetta, E., Canova, S., Lotze, M.T., Wesa, A., Parmiani, G., and Anichini, A. (2007). Interleukin-12: biological properties and clinical application. Clin. Cancer Res. *13*, 4677–4685. https://doi.org/10.1158/1078-0432.CCR-07-0776.
19. Cirella, A., Luri-Rey, C., di Trani, C.A., Teijeira, A., Olivera, I., Bolaños, E., Castañón, E., Palencia, B., Brocco, D., Fernández-Sendin, M., et al. (2022). Novel strategies exploiting interleukin-12 in cancer immunotherapy. Pharmacol. Ther. *239*, 108189. https://doi.org/10.1016/j.pharmthera.2022.108189.
20. Kerkar, S.P., Goldszmid, R.S., Muranski, P., Chinnasamy, D., Yu, Z., Reger, R.N., Leonardi, A.J., Morgan, R.A., Wang, E., Marincola, F.M., et al. (2011). IL-12 triggers a programmatic change in dysfunctional myeloid-derived cells within mouse tumors. J. Clin. Invest. *121*, 4746–4757. https://doi.org/10.1172/JCI58814.
21. Novick, D., Kim, S., Kaplanski, G., and Dinarello, C.A. (2013). Interleukin-18, more than a Th1 cytokine. Semin. Immunol. *25*, 439–448. https://doi.org/10.1016/j.smim.2013.10.014.
22. Drakes, D.J., Rafiq, S., Purdon, T.J., Lopez, A.V., Chandran, S.S., Klebanoff, C.A., and Brentjens, R.J. (2020). Optimization of T-cell receptor–modified T cells for cancer therapy. Cancer Immunol. Res. *8*, 743–755. https://doi.org/10.1158/2326-6066.CIR-19-0910.
23. Chaix, J., Tessmer, M.S., Hoebe, K., Fuséri, N., Ryffel, B., Dalod, M., Alexopoulou, L., Beutler, B., Brossay, L., Vivier, E., and Walzer, T. (2008). Cutting edge: priming of NK cells by IL-18. J. Immunol. *181*, 1627–1631. https://doi.org/10.4049/jimmunol.181.3.1627.
24. Cirella, A., Bolanos, E., Di Trani, C.A., de Andrea, C.E., Sánchez-Gregorio, S., Etxeberria, I., Gonzalez-Gomariz, J., Olivera, I., Brocco, D., Glez-Vaz, J., et al. (2022). Intratumoral gene transfer of mRNAs encoding interleukin-12 in combination with decoy-resistant interleukin-18 improves local and systemic antitumor immunity. Cancer Immunol. Res. CIR-22-0373. https://doi.org/10.1158/2326-6066.

25. Detry, S., Andries, J., Bloch, Y., Gabay, C., Clancy, D.M., and Savvides, S.N. (2022). Structural basis of human IL-18 sequestration by the decoy receptor IL-18 binding protein in inflammation and tumor immunity. J. Biol. Chem. *298*, 101908. https://doi.org/10.1016/j.jbc.2022.101908.

26. Zhou, T., Damsky, W., Weizman, O.-E., McGeary, M.K., Hartmann, K.P., Rosen, C.E., Fischer, S., Jackson, R., Flavell, R.A., Wang, J., et al. (2020). IL-18BP is a secreted immune checkpoint and barrier to IL-18 immunotherapy. Nature *583*, 609–614. https://doi.org/10.1038/s41586-020-2422-6.

27. Carbotti, G., Barisione, G., Orengo, A.M., Brizzolara, A., Airoldi, I., Bagnoli, M., Pinciroli, P., Mezzanzanica, D., Centurioni, M.G., Fabbi, M., and Ferrini, S. (2013). The IL-18 antagonist IL-18–binding protein is produced in the human ovarian cancer microenvironment. Clin. Cancer Res. *19*, 4611–4620. https://doi.org/10.1158/1078-0432.CCR-13-0568.

28. Hu, B., Ren, J., Luo, Y., Keith, B., Young, R.M., Scholler, J., Zhao, Y., and June, C.H. (2017). Augmentation of antitumor immunity by human and mouse CAR T cells secreting IL-18. Cell Rep. *20*, 3025–3033. https://doi.org/10.1016/j.celrep.2017.09.002.

29. Etxeberria, I., Bolaños, E., Quetglas, J.I., Gros, A., Villanueva, A., Palomero, J., Sánchez-Paulete, A.R., Piulats, J.M., Matias-Guiu, X., Olivera, I., et al. (2019). Intratumor adoptive transfer of IL-12 mRNA transiently engineered antitumor CD8+ T cells. Cancer Cell *36*, 613–629.e7. https://doi.org/10.1016/j.ccell.2019.10.006.

30. Melero, I., Castanon, E., Alvarez, M., Champiat, S., and Marabelle, A. (2021). Intratumoural administration and tumour tissue targeting of cancer immunotherapies. Nat. Rev. Clin. Oncol. *18*, 558–576. https://doi.org/10.1038/s41571-021-00507-y.

31. Cherkassky, L., Hou, Z., Amador-Molina, A., and Adusumilli, P.S. (2022). Regional CAR T cell therapy: an ignition key for systemic immunity in solid tumors. Cancer Cell *40*, 569–574. https://doi.org/10.1016/j.ccell.2022.04.006.

32. Majzner, R.G., Ramakrishna, S., Yeom, K.W., Patel, S., Chinnasamy, H., Schultz, L.M., Richards, R.M., Jiang, L., Barsan, V., Mancusi, R., et al. (2022). GD2-CAR T cell therapy for H3K27M-mutated diffuse midline gliomas. Nature *603*, 934–941. https://doi.org/10.1038/s41586-022-04489-4.

33. Brown, C.E., Alizadeh, D., Starr, R., Weng, L., Wagner, J.R., Naranjo, A., Ostberg, J.R., Blanchard, M.S., Kilpatrick, J., Simpson, J., et al. (2016). Regression of glioblastoma after chimeric antigen receptor T-cell therapy. N. Engl. J. Med. *375*, 2561–2569. https://doi.org/10.1056/NEJMoa1610497.

34. Adusumilli, P.S., Zauderer, M.G., Rivière, I., Solomon, S.B., Rusch, V.W., O'Cearbhaill, R.E., Zhu, A., Cheema, W., Chintala, N.K., Halton, E., et al. (2021). A phase I trial of regional mesothelin-targeted CAR T-cell therapy in patients with malignant pleural disease, in combination with the anti–PD-1 agent pembrolizumab. Cancer Discov. *11*, 2748–2763. https://doi.org/10.1158/2159-8290.CD-21-0407.

35. Overwijk, W.W., Theoret, M.R., Finkelstein, S.E., Surman, D.R., de Jong, L.A., Vyth-Dreese, F.A., Dellemijn, T.A., Antony, P.A., Spiess, P.J., Palmer, D.C., et al. (2003). Tumor regression and autoimmunity after reversal of a functionally tolerant state of self-reactive CD8+ T cells. J. Exp. Med. *198*, 569–580. https://doi.org/10.1084/jem.20030590.

36. Klebanoff, C.A., Finkelstein, S.E., Surman, D.R., Lichtman, M.K., Gattinoni, L., Theoret, M.R., Grewal, N., Spiess, P.J., Antony, P.A., Palmer, D.C., et al. (2004). IL-15 enhances the in vivo antitumor activity of tumor-reactive CD8 + T Cells. Proc. Natl. Acad. Sci. USA *101*, 1969–1974, –1974. https://doi.org/10.1073/pnas.0307298101.

37. Hildner, K., Edelson, B.T., Purtha, W.E., Diamond, M., Matsushita, H., Kohyama, M., Calderon, B., Schraml, B.U., Unanue, E.R., Diamond, M.S., et al. (2008). Batf3 deficiency reveals a critical role for CD8α + dendritic cells in cytotoxic T cell immunity. Science *322*, 1097–1100. https://doi.org/10.1126/science.1164206.

38. Woo, S.-R., Fuertes, M.B., Corrales, L., Spranger, S., Furdyna, M.J., Leung, M.Y.K., Duggan, R., Wang, Y., Barber, G.N., Fitzgerald, K.A., et al. (2014). STING-dependent cytosolic DNA sensing mediates innate immune recognition of immunogenic tumors. Immunity *41*, 830–842. https://doi.org/10.1016/j.immuni.2014.10.017.

39. Castle, J.C., Kreiter, S., Diekmann, J., Löwer, M., van de Roemer, N., de Graaf, J., Selmi, A., Diken, M., Boegel, S., Paret, C., et al. (2012). Exploiting the mutanome for tumor vaccination. Cancer Res. *72*, 1081–1091. https://doi.org/10.1158/0008-5472.CAN-11-3722.

40. Peng, L., Chen, Z., Chen, Y., Wang, X., and Tang, N. (2019). MIR155HG is a prognostic biomarker and associated with immune infiltration and immune checkpoint molecules expression in multiple cancers. Cancer Med. *8*, 7161–7173. https://doi.org/10.1002/CAM4.2583.

41. Sato, T., Terai, M., Tamura, Y., Alexeev, V., Mastrangelo, M.J., and Selvan, S.R. (2011). Interleukin 10 in the tumor microenvironment: a target for anticancer immunotherapy. Immunol. Res. *51*, 170–182. https://doi.org/10.1007/s12026-011-8262-6.

42. Riese, M.J., Wang, L.C.S., Moon, E.K., Joshi, R.P., Ranganathan, A., June, C.H., Koretzky, G.A., and Albelda, S.M. (2013). Enhanced effector responses in activated CD8+ T cells deficient in diacylglycerol kinases. Cancer Res. *73*, 3566–3577. https://doi.org/10.1158/0008-5472.CAN-12-3874.

43. Pearce, E.L., Mullen, A.C., Martins, G.A., Krawczyk, C.M., Hutchins, A.S., Zediak, V.P., Banica, M., DiCioccio, C.B., Gross, D.A., Mao, C.A., et al. (2003). Control of effector CD8 + T cell function by the transcription factor eomesodermin. Science *302*, 1041–1043. https://doi.org/10.1126/science.1090148.

44. Intlekofer, A.M., Takemoto, N., Wherry, E.J., Longworth, S.A., Northrup, J.T., Palanivel, V.R., Mullen, A.C., Gasink, C.R., Kaech, S.M., Miller, J.D., et al. (2005). Effector and memory CD8+ T cell fate coupled by T-bet and eomesodermin. Nat. Immunol. *6*, 1236–1244. https://doi.org/10.1038/ni1268.

45. Van den Steen, P., Rudd, P.M., Dwek, R.A., and Opdenakker, G. (1998). Concepts and principles of O-linked glycosylation. Crit. Rev. Biochem. Mol. Biol. *33*, 151–208. https://doi.org/10.1080/10409239891204198.

46. Fuhlbrigge, R.C., King, S.L., Sackstein, R., and Kupper, T.S. (2006). CD43 is a ligand for E-selectin on CLA+ human T cells. Blood *107*, 1421–1426. https://doi.org/10.1182/blood-2005-05-2112.

47. Matsumoto, M., Atarashi, K., Umemoto, E., Furukawa, Y., Shigeta, A., Miyasaka, M., and Hirata, T. (2005). CD43 functions as a ligand for E-selectin on activated T cells. J. Immunol. *175*, 8042–8050. https://doi.org/10.4049/jimmunol.175.12.8042.

48. Croci, D.O., Cerliani, J.P., Dalotto-Moreno, T., Méndez-Huergo, S.P., Mascanfroni, I.D., Dergan-Dylon, S., Toscano, M.A., Caramelo, J.J., García-Vallejo, J.J., Ouyang, J., et al. (2014). Glycosylation-dependent lectin-receptor interactions preserve angiogenesis in anti-VEGF refractory tumors. Cell *156*, 744–758. https://doi.org/10.1016/j.cell.2014.01.043.

49. Foxall, C., Watson, S.R., Dowbenko, D., Fennie, C., Lasky, L.A., Kiso, M., Hasegawa, A., Asa, D., and Brandley, B.K. (1992). The three members of the selectin receptor family recognize a common carbohydrate epitope, the sialyl Lewis(x) oligosaccharide. J. Cell Biol. *117*, 895–902. https://doi.org/10.1083/jcb.117.4.895.

50. Lawrence, M.B., and Springer, T.A. (1993). Neutrophils roll on E-selectin. J. Immunol. *151*, 6338–6346.

51. Abbassi, O., Kishimoto, T.K., McIntire, L.V., Anderson, D.C., and Smith, C.W. (1993). E-selectin supports neutrophil rolling in vitro under conditions of flow. J. Clin. Invest. *92*, 2719–2730. https://doi.org/10.1172/JCI116889.

52. Kolumam, G.A., Thomas, S., Thompson, L.J., Sprent, J., and Murali-Krishna, K. (2005). Type I interferons act directly on CD8 T cells to allow clonal expansion and memory formation in response to viral infection. J. Exp. Med. *202*, 637–650. https://doi.org/10.1084/jem.20050821.

53. Doulabi, H., Masoumi, E., Rastin, M., Foolady Azarnaminy, A., Esmaeili, S.-A., and Mahmoudi, M. (2022). The role of Th22 cells, from tissue repair to cancer progression. Cytokine *149*, 155749. https://doi.org/10.1016/j.cyto.2021.155749.

54. Hailemichael, Y., Johnson, D.H., Abdel-Wahab, N., Foo, W.C., Bentebibel, S.-E., Daher, M., Haymaker, C., Wani, K., Saberian, C., Ogata, D., et al. (2022). Interleukin-6 blockade abrogates immunotherapy toxicity and

promotes tumor immunity. Cancer Cell *40*, 509–523.e6. https://doi.org/10.1016/j.ccell.2022.04.004.

55. Naing, A., Infante, J.R., Papadopoulos, K.P., Chan, I.H., Shen, C., Ratti, N.P., Rojo, B., Autio, K.A., Wong, D.J., Patel, M.R., et al. (2018). PEGylated IL-10 (pegilodecakin) induces systemic immune activation, CD8+ T cell invigoration and polyclonal T cell expansion in cancer patients. Cancer Cell *34*, 775–791.e3. https://doi.org/10.1016/j.ccell.2018.10.007.
56. Mocellin, S., Marincola, F.M., and Young, H.A. (2005). Interleukin-10 and the immune response against cancer: a counterpoint. J. Leukoc. Biol. *78*, 1043–1051. https://doi.org/10.1189/jlb.0705358.
57. Ji, Y., and Gattinoni, L. (2015). miR-155 releases the brakes on antitumor T cells. Oncolmmunology *4*, e1026533. https://doi.org/10.1080/2162402X.2015.1026533.
58. Condé, C., Gloire, G., and Piette, J. (2011). Enzymatic and non-enzymatic activities of SHIP-1 in signal transduction and cancer. Biochem. Pharmacol. *82*, 1320–1334. https://doi.org/10.1016/j.bcp.2011.05.031.
59. Yang, J.C., and Rosenberg, S.A. (2016). Adoptive T-cell therapy for cancer. In Advances in immunology (Academic Press), pp. 279–294. https://doi.org/10.1016/bs.ai.2015.12.006.
60. Fernandez-Poma, S.M., Salas-Benito, D., Lozano, T., Casares, N., Riezu-Boj, J.-I., Mancheño, U., Elizalde, E., Alignani, D., Zubeldia, N., Otano, I., et al. (2017). Expansion of tumor-infiltrating CD8 + T cells expressing PD-1 improves the efficacy of adoptive T-cell therapy. Cancer Res. *77*, 3672–3684. https://doi.org/10.1158/0008-5472.CAN-17-0236.
61. Conde, E., Vercher, E., Soria-Castellano, M., Suarez-Olmos, J., Mancheño, U., Elizalde, E., Rodriguez, M.L., Glez-Vaz, J., Casares, N., Rodríguez-García, E., et al. (2021). Epitope spreading driven by the joint action of CART cells and pharmacological STING stimulation counteracts tumor escape via antigen-loss variants. J. Immunother. Cancer *9*, e003351. https://doi.org/10.1136/jitc-2021-003351.
62. Tselikas, L., Champiat, S., Sheth, R.A., Yevich, S., Ammari, S., Deschamps, F., Farhane, S., Roux, C., Susini, S., Mouraud, S., et al. (2021). Interventional radiology for local immunotherapy in oncology. Clin. Cancer Res. *27*, 2698–2705. https://doi.org/10.1158/1078-0432.CCR-19-4073.
63. Sun, R., Gao, D.S., Shoush, J., and Lu, B. (2022). The IL-1 family in tumorigenesis and antitumor immunity. Semin. Cancer Biol. *86*, 280–295. https://doi.org/10.1016/j.semcancer.2022.05.002.
64. Jaime-Sanchez, P., Uranga-Murillo, I., Aguilo, N., Khouili, S.C., Arias, M.A., Sancho, D., and Pardo, J. (2020). Cell death induced by cytotoxic CD8 + T cells is immunogenic and primes caspase-3–dependent spread immunity against endogenous tumor antigens. J. Immunother. Cancer *8*, e000528. https://doi.org/10.1136/jitc-2020-000528.
65. Minute, L., Teijeira, A., Sanchez-Paulete, A.R., Ochoa, M.C., Alvarez, M., Otano, I., Etxeberrria, I., Bolaños, E., Azpilikueta, A., Garasa, S., et al. (2020). Cellular cytotoxicity is a form of immunogenic cell death. J. Immunother. Cancer *8*, e000325. https://doi.org/10.1136/jitc-2019-000325.
66. Sánchez-Paulete, A.R., Teijeira, A., Cueto, F.J., Garasa, S., Pérez-Gracia, J.L., Sánchez-Arráez, A., Sancho, D., and Melero, I. (2017). Antigen cross-presentation and T-cell cross-priming in cancer immunology and immunotherapy. Ann. Oncol. *28*, xii44–xii55. https://doi.org/10.1093/annonc/mdx237.
67. van Kooyk, Y., and Rabinovich, G.A. (2008). Protein-glycan interactions in the control of innate and adaptive immune responses. Nat. Immunol. *9*, 593–601. https://doi.org/10.1038/ni.f.203.
68. Aires, D.J., Yoshida, M., Richardson, S.K., Bai, M., Liu, L., Moreno, R., Lazar, A.J.F., Wick, J.A., Rich, B.E., Murphy, G., et al. (2019). T-cell trafficking plays an essential role in tumor immunity. Lab. Invest. *99*, 85–92. https://doi.org/10.1038/s41374-018-0124-6.
69. Hervas-Stubbs, S., Mancheño, U., Riezu-Boj, J.-I., Larraga, A., Ochoa, M.C., Alignani, D., Alfaro, C., Morales-Kastresana, A., Gonzalez, I., Larrea, E., et al. (2012). CD8 T cell priming in the presence of IFN-α renders CTLs with improved responsiveness to homeostatic cytokines and recall antigens: important traits for adoptive T cell therapy. J. Immunol. *189*, 3299–3310. https://doi.org/10.4049/jimmunol.1102495.
70. Waldmann, T.A., Dubois, S., Miljkovic, M.D., and Conlon, K.C. (2020). IL-15 in the combination immunotherapy of cancer. Front. Immunol. *11*, 868. https://doi.org/10.3389/fimmu.2020.00868.
71. Davey, G.M., Starr, R., Cornish, A.L., Burghardt, J.T., Alexander, W.S., Carbone, F.R., Surh, C.D., and Heath, W.R. (2005). SOCS-1 regulates IL-15–driven homeostatic proliferation of antigen-naive CD8 T cells, limiting their autoimmune potential. J. Exp. Med. *202*, 1099–1108. https://doi.org/10.1084/jem.20050003.
72. Dudda, J.C., Salaun, B., Ji, Y., Palmer, D.C., Monnot, G.C., Merck, E., Boudousquie, C., Utzschneider, D.T., Escobar, T.M., Perret, R., et al. (2013). MicroRNA-155 is required for effector cd8+ t cell responses to virus infection and cancer. Immunity *38*, 742–753. https://doi.org/10.1016/j.immuni.2012.12.006.
73. Møller, S.H., Hsueh, P.-C., Yu, Y.-R., Zhang, L., and Ho, P.-C. (2022). Metabolic programs tailor T cell immunity in viral infection, cancer, and aging. Cell Metab. *34*, 378–395. https://doi.org/10.1016/j.cmet.2022.02.003.
74. Kawalekar, O.U., O'Connor, R.S., Fraietta, J.A., Guo, L., McGettigan, S.E., Posey, A.D., Patel, P.R., Guedan, S., Scholler, J., Keith, B., et al. (2016). Distinct signaling of coreceptors regulates specific metabolism pathways and impacts memory development in CAR T cells. Immunity *44*, 380–390. https://doi.org/10.1016/j.immuni.2016.01.021.
75. Teijeira, A., Garasa, S., Etxeberria, I., Gato-Cañas, M., Melero, I., and Delgoffe, G.M. (2019). Metabolic consequences of T-cell costimulation in anticancer immunity. Cancer Immunol. Res. *7*, 1564–1569. https://doi.org/10.1158/2326-6066.CIR-19-0115.
76. Labiano, S., Palazon, A., and Melero, I. (2015). Immune response regulation in the tumor microenvironment by hypoxia. Semin. Oncol. *42*, 378–386. https://doi.org/10.1053/j.seminoncol.2015.02.009.
77. Engelhardt, J.J., Boldajipour, B., Beemiller, P., Pandurangi, P., Sorensen, C., Werb, Z., Egeblad, M., and Krummel, M.F. (2012). Marginating dendritic cells of the tumor microenvironment cross-present tumor antigens and stably engage tumor-specific T cells. Cancer Cell *21*, 402–417. https://doi.org/10.1016/j.ccr.2012.01.008.
78. Zitvogel, L., and Kroemer, G. (2014). CD103+ dendritic cells producing interleukin-12 in anticancer immunosurveillance. Cancer Cell *26*, 591–593. https://doi.org/10.1016/j.ccell.2014.10.008.
79. Martínez-Sabadell, A., Arenas, E.J., and Arribas, J. (2022). IFNγ signaling in natural and therapy-induced antitumor responses. Clin. Cancer Res. *28*, 1243–1249. https://doi.org/10.1158/1078-0432.CCR-21-3226.
80. Paschen, A., Melero, I., and Ribas, A. (2022). Central role of the antigen-presentation and interferon-γ pathways in resistance to immune checkpoint blockade. Annu. Rev. Cancer Biol. *6*, 85–102. https://doi.org/10.1146/annurev-cancerbio-070220-111016.
81. Rožman, P., and Švajger, U. (2018). The tolerogenic role of IFN-γ. Cytokine Growth Factor Rev. *41*, 40–53. https://doi.org/10.1016/j.cytogfr.2018.04.001.
82. Fisher, D.T., Chen, Q., Skitzki, J.J., Muhitch, J.B., Zhou, L., Appenheimer, M.M., Vardam, T.D., Weis, E.L., Passanese, J., Wang, W.-C., et al. (2011). IL-6 trans-signaling licenses mouse and human tumor microvascular gateways for trafficking of cytotoxic T cells. J. Clin. Invest. *121*, 3846–3859. https://doi.org/10.1172/JCI44952.
83. Haas, A.R., Tanyi, J.L., O'Hara, M.H., Gladney, W.L., Lacey, S.F., Torigian, D.A., Soulen, M.C., Tian, L., McGarvey, M., Nelson, A.M., et al. (2019). Phase I study of lentiviral-transduced chimeric antigen receptor-modified T cells recognizing mesothelin in advanced solid cancers. Mol. Ther. *27*, 1919–1929. https://doi.org/10.1016/j.ymthe.2019.07.015.
84. Di Trani, C.A., Cirella, A., Arrizabalaga, L., Bella, Á., Fernandez-Sendin, M., Russo-Cabrera, J.S., Gomar, C., Olivera, I., Bolaños, E., González-Gomariz, J., et al. (2023). Intracavitary adoptive transfer of IL-12 mRNA-engineered tumor-specific CD8 + T cells eradicates peritoneal metastases in

mouse models. OncoImmunology *12*, 2147317. https://doi.org/10.1080/2162402X.2022.2147317.

85. Weigelin, B., Bolaños, E., Teijeira, A., Martinez-Forero, I., Labiano, S., Azpilikueta, A., Morales-Kastresana, A., Quetglas, J.I., Wagena, E., Sánchez-Paulete, A.R., et al. (2015). Focusing and sustaining the antitumor CTL effector killer response by agonist anti-CD137 mAb. Proceedings of the National Academy of Sciences *112*, 7551–7556. https://doi.org/10.1073/pnas.1506357112.

86. Bolger, A.M., Lohse, M., and Usadel, B. (2014). Trimmomatic: a flexible trimmer for Illumina sequence data. Bioinformatics *30*, 2114–2120. https://doi.org/10.1093/bioinformatics/btu170.

87. Dobin, A., Davis, C.A., Schlesinger, F., Drenkow, J., Zaleski, C., Jha, S., Batut, P., Chaisson, M., and Gingeras, T.R. (2013). STAR: ultrafast universal RNA-seq aligner. Bioinformatics *29*, 15–21. https://doi.org/10.1093/bioinformatics/bts635.

88. Liao, Y., Smyth, G.K., and Shi, W. (2014). featureCounts: an efficient general purpose program for assigning sequence reads to genomic features. Bioinformatics *30*, 923–930. https://doi.org/10.1093/bioinformatics/btt656.

89. Vijayasaradhi, S., Xu, Y., Bouchard, B., and Houghton, A.N. (1995). Intracellular sorting and targeting of melanosomal membrane proteins: identification of signals for sorting of the human brown locus protein, gp75. J. Cell Biol. *130*, 807–820. https://doi.org/10.1083/JCB.130.4.807.

90. Huber, W., Carey, V.J., Gentleman, R., Anders, S., Carlson, M., Carvalho, B.S., Bravo, H.C., Davis, S., Gatto, L., Girke, T., et al. (2015). Orchestrating high-throughput genomic analysis with Bioconductor. Nat. Methods *12*, 115–121. https://doi.org/10.1038/nmeth.3252.

STAR★METHODS

KEY RESOURCES TABLE

REAGENT or RESOURCE	SOURCE	IDENTIFIER
Antibodies		
Anti-mouse CD3	BioLegend	Clone 17A2; Cat# 100223; RRID: AB_312877
Anti-mouse CD28	BioLegend	Clone 37.51; Cat# 102112; RRID. AB:389326
Anti-mouse CD8 BV510	BioLegend	Clone 53–6.7; Cat# 100751; RRID: AB_2561389
Anti-mouse CD8 AF647	BioLegend	Clone 53–6.7; Cat# 100724; RRID:AB_389326
Rat Anti-CD8 PE-Cy7	BD Biosciences	Clone:53–6.7; Cat#552877; RRID:AB_394506
Anti-CD137 (3H3) for *in vivo* use	BioXcell	Clone 3H3; Cat# BE0239; RRID:AB_2687721
Anti-mouse CD4 BV421	BioLegend	Clone GK1-5; Cat# 100438; RRID: AB_11203718
Anti-mouse IL-12/IL-23 p40 PE	BioLegend	Clon C15.6; Cat# 505204; RRID: AB_315368
Anti-mouse IFNγ for *in vivo* use	BioXcell	Clone XMG1.2; Cat# E0055; RRID:AB_1107694
Anti-mouse IFNγ AF647	BioLegend	Clone XMG1.2; Cat# 505814; RRID:AB_493314
Anti-mouse IFN-gamma BV785	BioLegend	Clone: XMG1.2; Cat#505838; RRID:AB_2629667
Anti-mouse CD279 (PD1) FITC	BioLegend	Clone 29F.1A12; Cat# 135214; RRID:AB_10680238
Anti-SHIP1	Cell Signaling Technology	Polyclonal; Cat# 2728; RRID:AB_2126244
Anti-βactin	Sigma-Aldrich	Polyclonal; Cat# A2066; RRID:AB_476693
PE anti-mouse CD43 Activation associated glycoform	BioLegend	Clone 1B11; Cat# 121207; RRID:AB_493389
Anti-mouse affinity purified IL-22	R and D Systems	Polyclonal; Cat# AF582, RRID:AB_355457
InVivoMAb anti-mouse E-selectin (CD62E)	BioXCell	Clone 9A9; Cat#BE0294; RRID:AB_2687816
Rb mAb to Hexokinase II AF647	abcam	Cat#ab237314
TOX monoclonal antibody, PE, eBioscience	Thermo Fisher Scientific	Clone: TCRX10; Cat#12-6502-80; RRID:AB_10853657
Anti-mouse CD25 APC	BioLegend	Clone: PC61; Cat#102012; RRID: AB_312861
Anti-mouse CD137 BV421	BD Biosciences	Clone: 1AH2; Cat#740033; RRID:AB_2739805
Granzyme B monoclonal antibody, FITC, eBioscience	Thermo Fisher Scientific	Clone: NGZB; Cat#11-8898-82; RRID:AB_10733414
Anti-mouse Ki-67 Alexa Fluor® 700	BioLegend	Clone: 16A8; Cat#652420; RRID:AB_2564285
Anti-Rat CD90/mouse CD90.1(Thy-1.1) BV510	BioLegend	Clone: OX-7; Cat#202535; RRID:AB_2562643
Anti-mouse CD90.2 (Thy1.2) BV605	BioLegend	Clone: 30-H12; Cat#105343; RRID:AB_2632889
Active Caspase-3 PE	BD Bioscience	Clone: C92-605; Cat#550914; RRID:AB_393957
Bacterial and virus strains		
ElectroMAX™ DH10B	Invitrogen	Cat#18290015
Chemicals, peptides, and recombinant proteins		
Recombinant human IL-2 (Proleukin)	Novartis	Cat#CN70389
Percoll	GE Healthcare	Cat#17-0891-01
Recombinant mouse IL-7	Immunotools	Cat#12340075
Recombinant mouse IL-15	Immunotools	Cat#12340155
Recombinant mouse E-selectin-Fc	BioLegend	Cat#755504
Recombinant human TNFα	Peprotech	Cat#210-TA-020
Cytofix/Cytoperm fixation permeabilization kit	BD Biosciences	Cat#554714
CellTracker Orange CMRA Dye	Invitrogen	Cat#C34551
CellTracker Green CMFDA Dye	Invitrogen	Cat#C7025
7AAD Viability staining solution	BioLegend	Cat#79993
Zombi NIR Fixable viability Kit	BioLegend	Cat#54-423-106
Mitotracker green	ThermoFisher	Cat#M7514

(*Continued on next page*)

Continued

REAGENT or RESOURCE	SOURCE	IDENTIFIER
Mitochondrial Membrane Potential Kit (TMRM)	Merck	Cat#MAK159-1KT
hgp100 (25–33) peptide	Genscript	Cat#RP20344
OVA (257–264) peptide	Invivogen	Cat#vac-sin
DNAse I	Merck	Cat#1128493001
HindIII digestion enzyme	New England Biolabs	Cat#R0104S
Benzyl-α-GalNAc	Sigma-Aldrich	Cat#200100
2-NBDG	Cayman	Cat# 186689-07-6
Collagenase-D	Roche	Cat#11088866001
Ficoll Paque	Fisher Scientific	Cat#17144003
Lectin kit I-Fluorescein	Vector labs	Cat# FLK-2100
Lectin kit II-Biotinylated	Vector labs	Cat# BK-2100
AAL lectin-Biotinylated	Vector labs	Cat# B-1395-1
Protamine-sulfate	Sigma-Aldrich	Cat#P4020
M-MLV	Invitrogen	Cat#28025-013
iQ™ SYBR® Green Supermix	BIO-RAD	Cat#170-8882
Ringer Lactado	Grifols	Cat#637066
Critical commercial assays		
Mouse CD8+ T cell isolation kit	Miltenyi Biotech	Cat#130-104-075
T7 mScript™ Standard mRNA Production System	CellScript	Cat#C-MSC100625
RNeasy Micro Kit	Qiagen	Cat#74004
Endofree plasmid maxi kit	Qiagen	Cat#50912362
mouse IFNγ OptEIA set	BD Biosciences	Cat#551866
Mouse IL-12 (p70) ELISA set	BD Biosciences	Cat#555256
ELISA Mouse Duoset IL22	R and D Systems	Cat#DY582-05
Mouse ProcartaPlex Mix&Match 13-plex	Thermofisher	Cat#PPX-13MX2W9XU
Maxwell RSC simplyRNA tissue	Promega	Cat#AS1340
Deposited data		
RNAseq data	This paper	GEO: GSE206195
Experimental models: Cell lines		
Mouse: MC38	In house	N/A
Mouse: B16OVA	In house (Weigelin et al., 2015)[85]	N/A
Mouse B16F10	In house (Weigelin et al., 2015)[85]	N/A
Mouse: B16OVAgp75	In house (Weigelin et al., 2015)[85]	N/A
Mouse: MS-1	ATCC	RRID:CVCL_6502
Experimental models: Organisms/strains		
Mouse: C57BL/6	Envigo	Strain: C57BL/6JOlaHsd
Mouse Pmel1 TCR transgenic	Jackson Laboratory	Strain: 005023
Mouse: BATF3$^{-/-}$ on C57BL/6 background	In house	N/A
Mouse: CD45.1 on C57BL/6 background	In house	N/A
Mouse: OT-I TCR transgenic	Jackson Laboratory	Strain: 003831
Oligonucleotides		
Mouse single-chain IL-12 mRNA	In house (Etxeberria et al., 2019)[29]	N/A
Mouse IL-18 mRNA	This paper	N/A
Mouse DRIL18 mRNA	(Zhou et al., 2020)[26]	N/A
Mir155 mouse primers	This paper	N/A
Inpp5d (SHIP) mouse primers	This paper	N/A

(*Continued on next page*)

Continued		
REAGENT or RESOURCE	SOURCE	IDENTIFIER
miRCURY LNA™ miRNA Power Inhibitor Control. Negative control A	Qiagen	Cat#339136 YI00199006-DDA
miRCURY LNA™ miRNA Power Inhibitor MMU-MIR-155-5P	Qiagen	Cat#339131 YI04101319-DDA
Recombinant DNA		
pRubiC- EGFP-P2A-CAR retroviral vector	In house (Conde et al., 2021)[61]	N/A
Software and algorithms		
Prism 8	GraphPad Prism	https://www.graphpad.com; RRID:SCR_002798
FlowJo V10	Tree Star Inc.	https://www.flowjo.com/solutions/flowjo; RRID:SCR_008520
CytExpert Software	Beckman Coulter	https://www.mybeckman.com.br/flow-cytometry/research-flow-cytometers/cytoflex/software RRID:SCR_017217
RTCA Software	ACEA Biosciences Inc.	https://aceabio.com/product/rtca-dp/; RRID:SCR_014821
Imaris 9	Bitplane	http://www.bitplane.com/imaris/imaris; RRID:SCR_007370
R (v4.1.1)	Bioconductor	https://www.bioconductor.org; RRID:SCR_006442
FastQC tool (v0.11.9)	Babraham Bioinformatics	http://www.bioinformatics.bbsrc.ac.uk/projects/fastqc; RRID:SCR_014583
Trimmomatic (v.0.39)	(Bolger et al., 2014)[86]	http://www.usadellab.org/cms/?page=trimmomatic; RRID:SCR_011848
STAR (v. 2.7.9a)	(Dobin et al., 2013)[87]	http://code.google.com/p/rna-star/; RRID:SCR_004463
featureCounts (v.2.0.0)	(Liao et al., 2014)[88]	http://bioinf.wehi.edu.au/featureCounts/; RRID:SCR_012919

RESOURCE AVAILABILITY

Lead contact

Further information and requests for resources and reagents should be directed to and will be fulfilled by the Lead Contact, Ignacio Melero (imelero@unav.es).

Materials availability

Mouse scIL-12 mRNA and mouse IL-18 mRNA generated in this study will be made available on request, but we may require a payment and/or a completed Materials Transfer Agreement if there is potential for commercial application. The mouse lines generated in this study are available upon request.

Data and code availability

- Bulk RNAseq data have been deposited in GEO and are publicly available as of the date of publication. Accession numbers are listed in the key resources table.
- This paper does not generate custom code. The code used for the RNA-seq analysis is available upon request.
- Any additional information required to re-analyze the data reported in this paper is available from the lead contact upon request.

EXPERIMENTAL MODEL AND SUBJECT DETAILS

Mice

All mouse procedures were approved by the ethics committee for animal experimentation of the regional Government of Navarra under Spanish regulations (study 079/20). Mice were housed at the animal facility of the Center for Applied Medical Research (CIMA, Pamplona, Spain). Six week-old female C57BL/6 mice were purchased from Envigo (Barcelona, Spain). Pmel-1,[35] OT-I and Batf3$^{-/-}$gene-modified mice were bred in our facilities (CIMA, Pamplona, Spain). Batf3$^{-/-}$ mice were kindly provided to us by Dr. David Sancho (CNIC, Madrid, Spain).[37] Littermates of the same age (7-10-week-old) were randomly assigned to experimental groups.

Tumor cell lines

MC38 cells were a kind gift from Dr. Karl E. Hellström (University of Washington, Seattle, WA) in September 1998. B16-OVA cells were provided by Dr. Lieping Chen (Yale University, New Haven, CT) in November 2001. B16F10 cells were purchased from the ATCC in June 2006. Cell lines were cultured in complete media containing RPMI1640 medium (Gibco) supplemented with 10% FBS (Sigma-Aldrich), 100 IU/mL penicillin and 100 mg/mL streptomycin (Gibco) and 5x10-5 mol/L 2-mercaptoethanol (Gibco). B16-OVA cultures were supplemented with 400 mg/mL geneticin (Gibco). B16OVAgp75transfectants were generated by transduction of B16OVA cells with an amphotropic retrovirus coding a mutated gp75 (gp75δ27) lacking the last 27 amino acids necessary for intracellular sorting of gp75 into melanosomes and exhibiting enhanced surface expression.[89]

All cell lines were grown in a humidified incubator with 5% CO_2 at 37ºC for at least 7 days before inoculation to mice. All cell lines were routinely tested every 8 weeks for mycoplasma contamination using the MycoAlert Mycoplasma Detection Kit (Lonza).

Primary cells

All mouse primary lymphocytes were activated/expanded, as described in the method details section, in a humidified incubator with 5% CO_2 at 37ºC and cultured at a density of 1.5x10^6 cells/mL in complete media (RPMI1640 medium (Gibco) supplemented with 10% FBS (Sigma-Aldrich), 100 IU/mL penicillin and 100ug/mL streptomycin (Gibco) and 5x10-5 mol/L 2-mercaptoethanol (Gibco)).

METHOD DETAILS

Vector constructs, mRNA *in vitro* transcription and mRNA transduction by electroporation

The mouse scIL-12 mRNA, the mouse IL-18 mRNA and the mouse DRIL18 mRNA encoding cDNA sequences were cloned by GeneScript Inc. in pUC57-Kan vector holding a T7 promotor upstream of the cDNAs and followed by 2 tandem repetitions of the 3′UTR sequence of the human β2-Globin cDNA and a 120 poly A tail. DRIL18-encoding cDNA sequence was recently published.[26] The mRNA encoding sequences on the cloning vectors were confirmed by direct sequencing and linearized by HindIII enzyme (New England Biolabs) prior to RNA *in vitro* synthesis. T7mScript™ Standard mRNA Production System (Cellscript) was used to generate capped IVT RNA from the cloning vectors according to the manufacturer's instructions. The IVT RNA was purified using the RNeasy Mini Kit (Qiagen), and the purified mRNA was eluted in RNase-free water at 1–2 mg/mL.

For mRNA electroporation, the stimulated and expanded T cells were washed and resuspended in OPTI-MEM (Gibco) at a final concentration of 100 × 10^6 cells/mL. Subsequently, the cells were mixed with 10 μg of mRNA IVT per 0.1 mL and electroporated in 2 mm cuvettes (BioRad) using the Gene pulser Mx System (BioRad). T cell viability was checked 30 min after electroporation by flow cytometry using the Zombi NIR Fixable viability kit (BD biosistems).

Mouse lymphocyte isolation, activation and expansion

Pmel-1 and OT-I T cells were obtained from the spleen of Pmel-1 and OT-I mice respectively.[29] Pmel-1 splenocytes were activated 48 h with 100 ng/mL of hgp100 peptide (Genscript). For OT-I splenocyte activation, we performed 48h cultures with 1 ng/ml of OVA peptide (Invivogen). Polyclonal CD8$^+$ T cells were isolated with the CD8$^+$ T cell isolation kit (MiltenyiBiotec) by negative selection using manual columns and following the manufacturer's instructions. CD8$^+$ T cell purity after selection was routinely tested by flow cytometry. Polyclonal CD8$^+$ T cells were stimulated with plate-bound anti-CD3 mAb (2 μg/mL, clone 17A2, Biolegend) and supplemented with soluble anti-CD28 mAb (1 μg/mL, clone 37.51, Biolegend) for 48 h. For expansion, stimulated cells were incubated with 50 IU/mL of human IL-2 (Proleukin) for 48 h.

Retroviral transduction of mouse T cells

Retroviral generation was performed as previously reported.[61] Briefly, isolated CD8 T cells from splenocytes were activated in 24-well plates (Cellstar) coated with anti-CD3 mAb (2 μg/mL, clone 17A2, Biolegend) and supplemented with soluble anti-CD28 mAb (1 μg/mL, clone 37.51, Biolegend) for 48 h in complete medium supplemented with human IL-2 (50U/ml) (Proleukin) at 10^6/mL density. After 48 h later, lymphocytes were resuspended in retrovirus supernatant containing protamine sulfate (10 μg/mL, SIGMA) and human IL-2 and were spin-inoculated at 2000 x g for 90 min at 32°C. This process was repeated again with additional fresh retrovirus supernatant the next day. Then, CAR T cells were cultured at 37°C until day +7, electroporated with the indicated mRNAs to perform experiments. Transduction efficiency was checked by flow cytometry measuring reporter protein (EGFP) expression.

Mouse TIL isolation, sorting and expansion

TIL isolation, sorting and expansion were performed as previously described.[60] Briefly, 20-day established bilateral MC38 tumors were excised, minced and digested with 400 U/mL collagenase D and 50 μg/mL DNase-I (Roche). Donor mice had been treated with anti-CD137 (3H3) mAb on days +12 and +15 to enhance T cell infiltration of tumors. Living cells were enriched by Percoll 35% (Merck) gradient centrifugation and cultured overnight in mouse complete media supplemented with 25 ng/mL of recombinant murine IL-7 (Immunotools) and IL-15 (Immunotools). For sorting of $CD8^+$ PD1+ and $CD8^+$ PD1- TILs, cells were stained with 7AAD+ viability-staining solution (BioLegend), CD8-AF467 (Biolegend) and PD-1-FITC (Biolegend) mAbs and run in a FACSAria sorter (BD Biosciences). Sorted $CD8^+$ TILs were activated and expanded in culture with irradiated allosensitized allogeneic lymphocytes (ASAL) and BALB/c-derived allogenic bone marrow-derived DCs. For ASAL generation, C57/BL6 CD45.1 splenocytes were irradiated (4000 Rads) and cocultured with BALB/c splenocytes at a 1:1 ratio for 7 days in complete mouse media supplemented with 100 IU/mL of human recombinant IL-2 (Proleukin). ASALs were enriched by Ficoll Paque™ PLUS (GE Healthcare) centrifugation and were irradiated (4000 Rads) prior to co-culturing with TILs and DCs. For DC generation, BALB/c bone marrow cell suspensions were differentiated during 6 days in mouse complete media supplemented with 20 ng/mL of recombinant murine GM-CSF (Peprotech) and matured overnight with 1 mg/mL of LPS (Invivogen). For sorted TIL activation and expansion, TILs, ASALs, and DCs were cocultured over 10 days at a 1:4:1 ratio in mouse complete media supplemented with 1500 IU/mL of IL-2 (Proleukin) and soluble anti-CD3 (17A2, BioLegend) and anti-CD137 (3H3) mAbs at 100 ng/mL.

In vivo tumor inoculation, adoptive T cell transfer and treatments

For antitumor efficacy experiments, the B16-OVA tumor cell line was injected subcutaneously (0.5×10^6 cells in the right flank and 0.15×10^6 cells in the left flank) in 50 μL saline into 6–10 week old C57BL/6 or *Batf3*$^{-/-}$ mice on day 0. The resulting right tumors received intratumoral injections. For rechallenge experiments of tumor free surviving mice, 0.5×10^6 B16-OVA cells were injected in upper lateral flanks, distant from the site of the originally rejected tumor, at least 90 days following tumor rejections. For TIL extraction experiments, $0.5x10^6$ MC38 cells were subcutaneously injected bilaterally in 6-week-old C57BL/6 mice.

Adoptive T cell therapy (ACT) experiments were performed in tumor-bearing mice at the indicated time points by intratumoral (i.t.) or intravenous (i.v.) injection of 5×10^6 mRNA- or mock-electroporated Pmel-1 or OT-I, 10^6 TILs or 10^6 CAR T cells in 50μL of saline buffer. Vehicle-treated mice were injected intratumorally with 50 μL of saline buffer. For the experiment with "naked" mRNA, 5μg of each mRNA (IL-12 and DRIL18) were injected in 50μL of Ringer's lactate buffer (Grifols).

In vivo neutralization and inhibition experiments

For IFN-ɣ neutralization, mice were i.p. given 200μg of anti-IFN-ɣ (XMG1.2, BioXcell) or the matched isotype rat IgG1 (BioXcell) one day prior to ACT (corresponding to days +7 and +10), and twice during the following week after the second dose of ACT, days +13 and +16 for maintenance.

For E-selectin blockade, mice were injected i.v. with 90 μg of InViVoMAb anti-mouse E-selectin (9A9, BioXcell) starting the day of ACT until day +10. On day +11, tumors were collected and stained to determine the migration of the Pmel-1 cells to the contralateral tumor.

For the O-glycosylation inhibition, mRNA-electroporated Pmel-1 cells were cultured for 2h in the presence of i benzyl- α-GalNAc (2mM) (Sigma-Aldrich) before ACT.

For miR-155 inhibition experiments, Pmel-1 cells were co-electroporated with the corresponding mRNA and the miRCURY LNA miR-155 Inhibitor or negative control (1.5μM) (Qiagen) in the electroporation medium.

Adoptively transfer and endogenous T cell characterization

For lymphocyte characterization after ACT, B16-OVA tumors were collected 72h following one dose of mRNA-electroporated Pmel-1 cells and the corresponding cell suspensions were analyzed by flow cytometry.

For hexokinase-II expression analysis, B16-OVA bearing mice were treated with one dose of mRNA-electroporated Pmel-1 cells on day+8. 24h later, tumors were collected and assessed individually by flow cytometry. Averages of intensity of fluorence were studied for correlation with other markers.

Flow cytometry

For surface flow cytometry analyses, lymphocytes, CAR or TILs were treated with FcR-Block (anti-CD16/32 clone 2.4G2; BD Biosciences), and then surface stained with the following fluorochrome-labeled antibodies purchased from BioLegend: anti-CD4-BV421 (GK1.5), anti-CD8-BV510, -PE-Cy7 or -AF647 (53–6.7), anti-PD1-FITC (29F.1A12), anti-CD25-APC (PC61), anti-CD137-BV421 (1AH2), anti-CD90.1-BV510 (OX-7), anti-CD90.2-BV605 (30-H12) or/and anti-CD43 activation associated glycoform-PE (1B11). For intracellular staining, cells were permeabilized after surface staining with ice-cold Cytofix/Cytoperm (BD) for 10 min following the manufacturer's instructions and intracellularly stained with anti-IL12-p40-PE (C15.6), anti-IFN γ-AF647 or BV785 (XMG1.2), anti-hexokinase-II-AF647 and anti-GzmB-FITC (NGZB). For intranuclear staining, cells were permeabilized with True Nuclear Transcription Factor Buffer Set (BioLegend) for 40 min and stained with anti-Ki-67-AF700 (16A8), anti-TOX-PE (TCRX10) and active caspase-3-PE (C92-605).

For lectin staining, 48h-cultured Pmel-1 electroporated T cells were incubated 30 min at 4°C with plant lectins (Lectin kit I and II, Vector labs) and then co-labelled with anti-CD8 BV510 and anti-CD4 BV421.

The Zombi NIR Fixable viability kit (BioLegend) or 7AAD Viability Kit (BioLegend) were used as a live/dead marker. Flow cytometry was performed using CytoFLEX (Beckman Coulter) cytometer.

Serum toxicity determination

Serum ALP (alkaline phosphatase), AST (aspartate aminotransferase), CRP (C-reactive protein), LDH (lactate dehydrogenase) and IFNɣ levels were determined in peripheral blood samples of tumor bearing mice 48h after mRNA-electroporated Pmel-1 treatment corresponding to day +10 in the B16-OVA model. ALP, AST, CRP and LDH levels were determined using the Cobas c311 analyzer (Roche) and IFNɣ levels were assessed by mouse IFNγ OptEIA set (BD).

In vitro cytotoxicity assays (xCELLigence)

In vitro real-time killing assays were performed by measuring electric impedance over time in an xCELLigence Real Time Cell Analysis Instrument (ACEA). $5x10^3$ B16OVA cells were seeded onto a 16-well plate (ACEA) and cultured for 4 h prior to the assay thereby allowing tumor cell adhesion. After the 4h-culture, $1x10^3$ Pmel-1 T cells that had received the indicated electroporation conditions with or without miRCURY miR-155 Inhibitor or a similarly synthetized irrelevant negative control (1.5 μM) (Qiagen) were added to the B16-OVA containing wells, in a 1:5 target-effector ratio. When indicated, for IFN-ɣ and IL-22 neutralization we added 2.5 μg/mL of anti-IFN-ɣ (XMG1.2, BioXcell) or anti-IL22 (R&D). Electric impedance was measured every 5 min for 96 h.

Adhesion assays

For the adhesion assays, 96-well plates were coated overnight at 4°C with E-selectin-Fc diluted to 2 μg/mL in 100μL PBS per well. Pmel-1 activated CD8 T cells transfected 48 h prior to the experiment with either scIL-12 mRNA alone or mixed with DRIL18 electroporated cells were pre-stained with either CMRA Orange or CMFDA fluorescent probes and then mixed at $0.5x10^6$/mL in an eppendorf tube just before the experiment. Adhesion was measured following a 15-min incubation at 37ºC and 5% CO2. After this incubation period, plates were washed with PBS 5 times by inverting the plate. Then, we added 100 μL of 10% PFA to fixate the cells. After 30 min of incubation at 37ºC, plates were washed twice with PBS and kept at 4ºC. Differential adhesion was analyzed in confocal microscopy images. Microscopy was performed in an LSM 880 inverted microscope (Zeiss) using a 488 Argon Laser and a 561 nm laser lines and a 10x objective (Plan Neofluar 0.3 N/A). Quantification was carried out by counting differentially colored cells using IMARIS 9 software (Bitplane).

Flow adhesion assays

For the study of adhesion and arrest under flow conditions, IBIDI mSLIDE I (0.2 mm channel height) sticky slides were attached to glass cover glasses. E-selectin-Fc at 2 μg/mL in PBS was used to coat the glass surface for 16 h at RT. In other experiments the chambers were coated with collagen type 1 (1 mg/ml) and then $8x10^5$ endothelial MS1 cells were seeded. Twenty-four h later the endothelial cells were treated with 20 ng/mL TNF-α for an additional 16 h. Pmel-1 activated CD8 T cells mRNA-transduced 48 h earlier with either scIL-12 mRNA alone or in combination with DRIL18 electroporated-cells were pre-stained respectively with CMRA orange and CMFDA green fluorescent probes and then mixed at a density of $0.5x10^6$ cells/ml in DMEM containing HEPES 1 mM. Tubing was connected to the flow chambers establishing a closed circuit using a peristaltic pump (Senchen MC series). The shear flow was set up at 1.4 dyn/cm^2 following the manufacturer's instructions. Live imaging was performed in an LSM880 confocal microscope equipped with a heated staged and T cell media was also kept at 37°C. Single plane images focusing on the endothelial monolayer (or glass surface) were obtained every 500 ms under simultaneous excitation with 488 nm and 543 nm lasers using a 25x LD water immersion objective (N/A: 0.8). Videos were analyzed with IMARIS 9 (Bitplane) using automatic tracking algorithms.

Mitochondria staining

For mitochondria staining, cells were incubated with a mitochondrial transmembrane potential indicator (TMRM; 125 ng/mL, Sigma) and MitoTracker green (5 mmol/L; both from Thermo Fisher Scientific) in complete culture media for 20 min at 37°C and assessed in confocal microscopy images. Microscopy was performed in an LSM 880 inverted microscope (Zeiss) using a 488 Argon Laser and a 543 nm solid state laser and a 63x oil immersion objective (N/A 1.4).

Cytokine measurement in T-cell culture supernatants

For cytokine determination, we used 24 or 48 h-supernatants from Pmel-1 mRNA-electroporated T cells either with scIL-12 or DRIL18 mRNAs and then mixed 1:1 in comparison with single mRNA-transfected T cells. A mouse ProcartaPlex Mix&Match 13-plex (Thermofisher) was used to measure mouse IFN-γ, TNF-α, IL-15, IFN-α, IFN-β, CCL3, IL-10, IL-6 and IL-12 cytokines. Additionally, we used mouse IFNγ OptEIA set (BD), mouse IL-12 (p70) ELISA set and ELISA Mouse Duoset IL-22 for single measurements of IFN-γ, IL-12 and IL-22.

Seahorse and glucose uptake assays

For Seahorse assays, we electroporated Pmel-1 cells with scIL-12 or DRIL18 mRNAs and, when indicated, mixed prior to the experiment. Cells were resuspended in the assay medium (Seahorse XF DMEM medium pH 7.4 (Agilent) without phenol red supplemented with 15mM de glucose, 1 mM pyruvate and 2mM glutamine) and added to pre-coated XFs Microplates (Agilent) with Cell-Tak. Then, plates were centrifuged at 300 g for 1 min with no brake and placed in a non-CO_2 incubator at 37°C to equilibrate the temperature for 30 min. Microplates were placed into the Agilent Seahorse XF Analyzer (Agilent) to assess glucose metabolism and respiratory capacity by adding to the culture 1 μM oligomycin (Sigma); 2 μM FCCP (Sigma), 1μM Antimycin A/Rotenone (Sigma) and 75 mM 2-DG.

For the glucose uptake assays, T cells following a 1h-resting period in glucose-free medium were cultured with 150 μM of 2-NBDG probe at 37°C during 30 min. Then, cells were surface stained with anti-CD8 mAb BV510 and anti-CD4 mAb BV421 to be analyzed by conventional flow cytometry.

Western blots

Pmel-1 mRNA-electroporated T cells were electroporated with the corresponding mRNA and cultured for 48 h. After a 2-day culture, T cells were lysed with RIPA buffer (30mM HEPES, pH 7.4,150mM NaCl, 1% Nonidet P-40,0.5% sodium deoxycholate, 0.1% sodium dodecyl sulfate, 5mM EDTA, 1mM NaV04, 50mM NaF, 1mM PMSF, 10% pepstatin A, 10 μg/mL leupepsin, and 10 μg/mL aprotinin) on ice for 30 min and centrifuged for another 30 min at maximum speed. Supernatants were collected and the BCA kit (Themofisher) was used to analyzed protein concentrations. Western blots were performed in reducing conditions in polyacrylamide gels and blotted onto PVDF membranes. Pre-blocked membranes were incubated overnight with the primary antibodies (anti-SHIP-1 or anti-β-actin) in TBS supplemented with 5% of skimmed milk at 4°C. Following overnight incubation, membranes were washed with TBS 1% Tween 3 times and incubated for 4 h with the secondary-HRP antibody. Finally, we analyzed chemiluminescence using the Chemidoc Imagin System (BioRad). For densitometry measurements, ImageJ software was used.

RNA extraction and quantitative RT-PCR

Total RNA was extracted from Pmel-1 cells 24h after electroporation with the Maxwell RSC simplyRNA extraction kit (Promega), according to the manufacturer's instructions and subsequently retrotranscribed into cDNA using M-MLV enzyme kit (Invitrogen). Real-time PCR reactions were performed into Bio-rad CFX qPCR system with customized primers for mouse *Mir155hg (FW 5′-AAACCAGGAAGGGGAAGTGTG and Rv 5′-TAGGAGTCAGAGGCCAA), mouse Inpp5d* (FW 5′-TCCCCAGATCAGCAACTCAC and Rv 5′-CAGATCCCCAGGTCTTGCCT) and mouse Actb (FW 5′-CGCGTCCACCCGCGAG and Rv 5′-CCTGCCTAGGGCG).

RNAseq sample preparation and bioinformatic analysis

For transcriptomic analyses, we collected mixtures of Pmel-1 T cells electroporated 24 h before with scIL-12 or DRIL18. RNA was extracted using the RNA Easy Mini Kit (Qiagen) and sent to Macrogen (South Korea) to perform the RNAseq analysis.

All sample processing and subsequent bioinformatics analysis were performed on a workstation equipped with 16x Intel Xeon W-2245 @ 4.7 GHz and 256 GB of RAM in a Linux system (Ubuntu 20.04).

For the processing of RNA-Seq samples, quality control was performed with FastQC tool (v0.11.9) (http://www.bioinformatics.bbsrc.ac.uk/projects/fastqc). Before alignment, reads with low quality and adapters were removed using Trimmomatic (v.0.39).[86] Alignment was performed using STAR (v. 2.7.9a)[87] and the mm39 assembly used as a reference. The matrix of raw counts was obtained with featureCounts (v.2.0.0)[88] and annotated with Gencode version M27.

The analysis of differentially expressed genes was carried out in the R/Bioconductor (v4.1.1)[90] statistical environment. In brief, the TMM normalization method from the edgeR package (v.3.35) was independently applied to each dataset, and the log_2CPMs were obtained using voom, making the samples comparable. Before normalization, genes with fewer than 5 counts in all the samples (non-expressed genes) were removed from the analysis. We selected the set of differentially expressed genes for each comparison (adj.P.val< 0.05 and logFC $-1 < | > 1$). Gene Ontology enrichment analysis was performed with the DE genes of the scIL-12/DRIL18 condition versus scIL-12 using the clusterProfiler package (v.4.2.0) with the Biological Process ontology (GOBP) as reference. Gene Set enrichment analysis (GSEA) was performed with all the expressed genes ordered by their t-statistics using the fgsea package (v.1.20) against the M2 and M3 collections of MSigDB (https://www.gsea-msigdb.org/gsea/msigdb/mousegenesetresources.jsp) as references.

QUANTIFICATION AND STATISTICAL ANALYSES

Data were processed using GraphPad Prism 8.0. Flow cytometry analysis were performed with FlowJoV10 or CytExpert software. Means and standard errors of the mean or standard deviation are presented as averages and error bars. Tumor measurements in *in vivo* experiments are represented as tumor area (mm^2) and plotted either as individual datapoints for one individual mouse or as mean of tumor areas from a group of mice ±SEM. All *in vivo* experiments were performed at least twice with 6 mice per group unless otherwise indicated in the figure legends.

One-way ANOVA tests were used to analyze statistical differences between independent groups. For *in vivo* experiments, survival differences between experimental groups were analyzed by Log rank (Mantel-Cox) tests and differences in tumor growth by two-way ANOVA tests. Statistical significance is considered at $p < 0.05$. When differences are statistically significant, the significance is represented with asterisks (*) according the following values: $p < 0.05$(*), $p < 0.01$(**), $p < 0.001$(***) and $p < 0.0001$ (****).

Cell Reports Medicine, Volume *4*

Supplemental information

mRNAs encoding IL-12 and a decoy-resistant variant of IL-18 synergize to engineer T cells for efficacious intratumoral adoptive immunotherapy

Irene Olivera, Elixabet Bolaños, Jose Gonzalez-Gomariz, Sandra Hervas-Stubbs, Karina V. Mariño, Carlos Luri-Rey, Iñaki Etxeberria, Assunta Cirella, Josune Egea, Javier Glez-Vaz, Saray Garasa, Maite Alvarez, Iñaki Eguren-Santamaria, Sonia Guedan, Miguel F. Sanmamed, Pedro Berraondo, Gabriel A. Rabinovich, Alvaro Teijeira, and Ignacio Melero

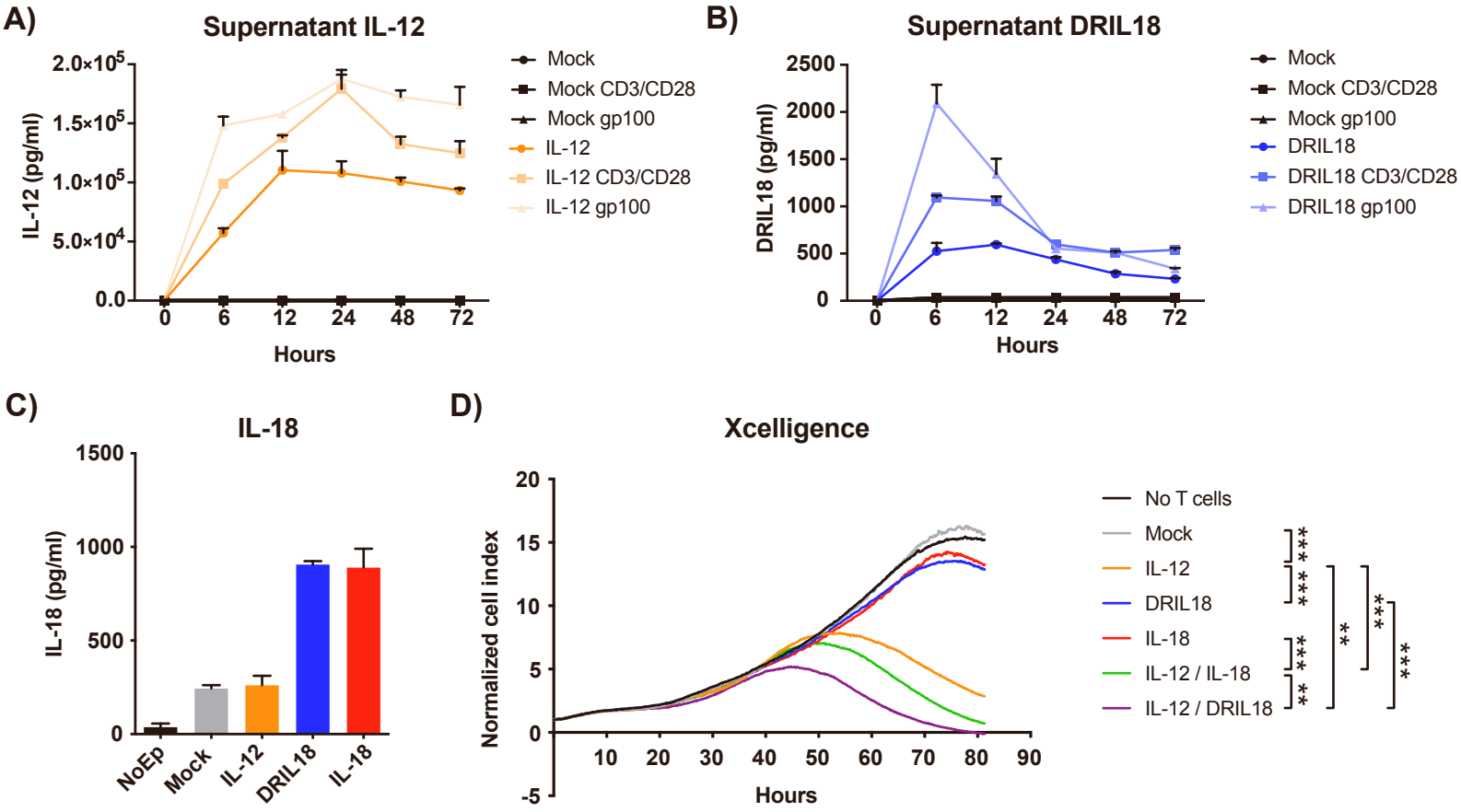

Figure S1. Electroporated mRNAs encoding IL-18, IL-12 and DRIL18 confer expression of these cytokines to Pmel-1 CD8 T lymphocytes and enhance their cytotoxic function. Related to Figure 1.

(A and B) Time course of IL-12 and DRIL18 concentrations in supernatants of pmel-1 cells electroporated with the indicated mRNAs. Pmel-1 cells were preactivated by cognate gp100 peptide and restimulated with CD3+CD28 or gp100 during the cultures.

(C) TCR-transgenic splenic Pmel-1 T cells activated by gp100 cognate peptide for 48h and maintained another 48h with IL-2 were transfected with in-vitro synthetized mRNAs encoding IL-12, DRIL18 and IL-18 concentrations in the supernatant were determined 48 h later.

(D) Cytotoxicity experiment with Pmel-1 electroporated with the indicated cytokine-encoding mRNAs that were cocultured with B16-OVA cells at 1:5 ratio. IL-12/IL-18 and IL-12/DRIL18 indicate Pmel-1 cells electroporated separately with each mRNA and mixed together one to one before the experiment.

Two-way ANOVA tests were used for comparisons. Experiments are representative of at least two similarly performed. Biological duplicates were performed in all experiments. Data is represented as mean +/- SD.

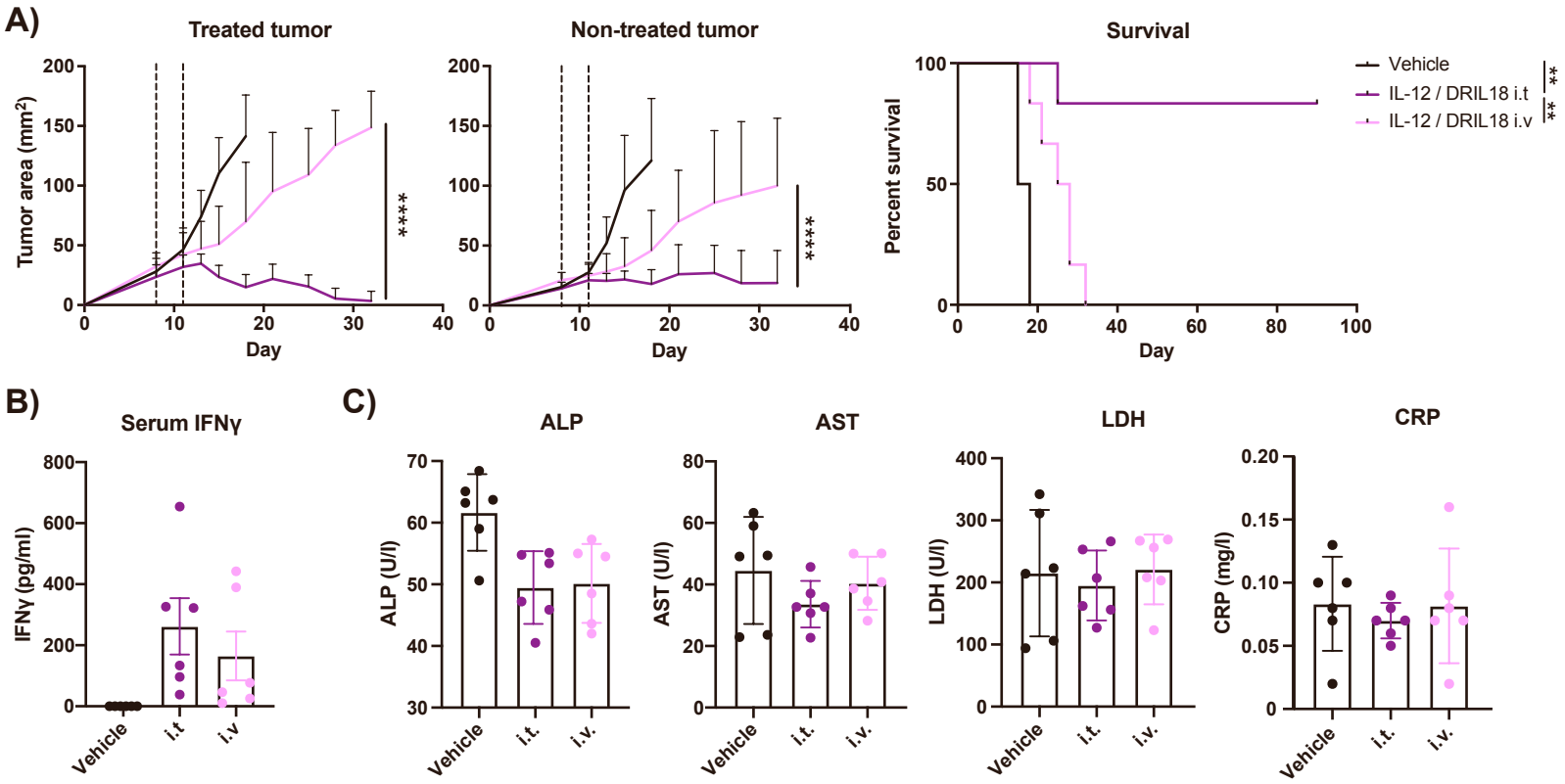

Figure S2. Unilateral intratumoral delivery is more efficacious than intravenous delivery in the B16OVA bilateral mouse model. Related to FIgure 1.

(A) Experiments as in figure 1H comparing intratumoral versus intravenous delivery of identical doses of IL-12/DRIL18 electroporated pmel-1 cells.

(B) Concentrations of IFNγ in the serum of treated mice 48h after the second T-cell dose given intravenously or intratumorally as indicated.

(C) Concentrations of ALP (alkaline phosphatase), AST (aspartate aminotransferase) LDH (lactate dehydrogenase) and CRP (C-reactive protein) in the serum of treated mice 48h following the second dose given as indicated.

Statistical comparisons were performed using two-way ANOVA and log-rank test. Experiments are representative of two similarly performed. For each experiment, we randomly assigned 6 mice per group. Data is represented as mean +/- SD.

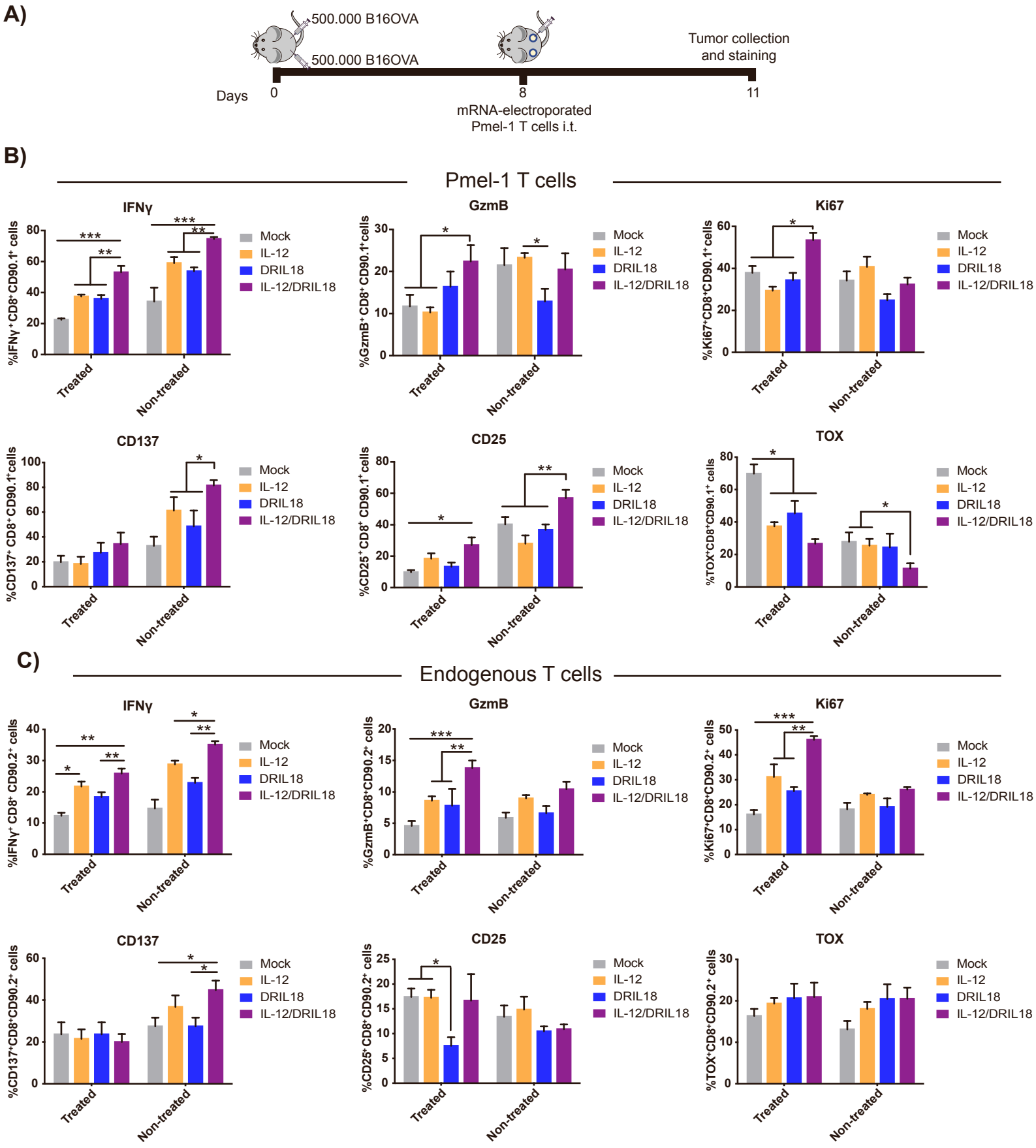

Figure S3. Adoptively transferred cells upon IL-12/DRIL18 mRNA electroporation show stronger signs of proliferation and activation. Related to Figure 1.

(A) Schematic representation of the experiments. At the end of the experiment, the directly injected and contralateral tumors were collected and a multicolor flow cytometry was performed on cell suspensions electronically gating CD90.1+ adoptively transferred ells and endogenous CD90.2+ CD8+ T lymphocytes.

(B) Percentages of expression of the indicated markers in pmel-1 cells that had been electroporated with the indicated mRNAs. (

C) Similar determination in the tumor-infiltrating CD8 T-cell compartment. Statistical comparisons were performed using one-way ANOVA tests. Experiments are representative of two similarly performed. We randomly assigned 6 mice per group before tumor injection. Data is represented as mean +/- SD.

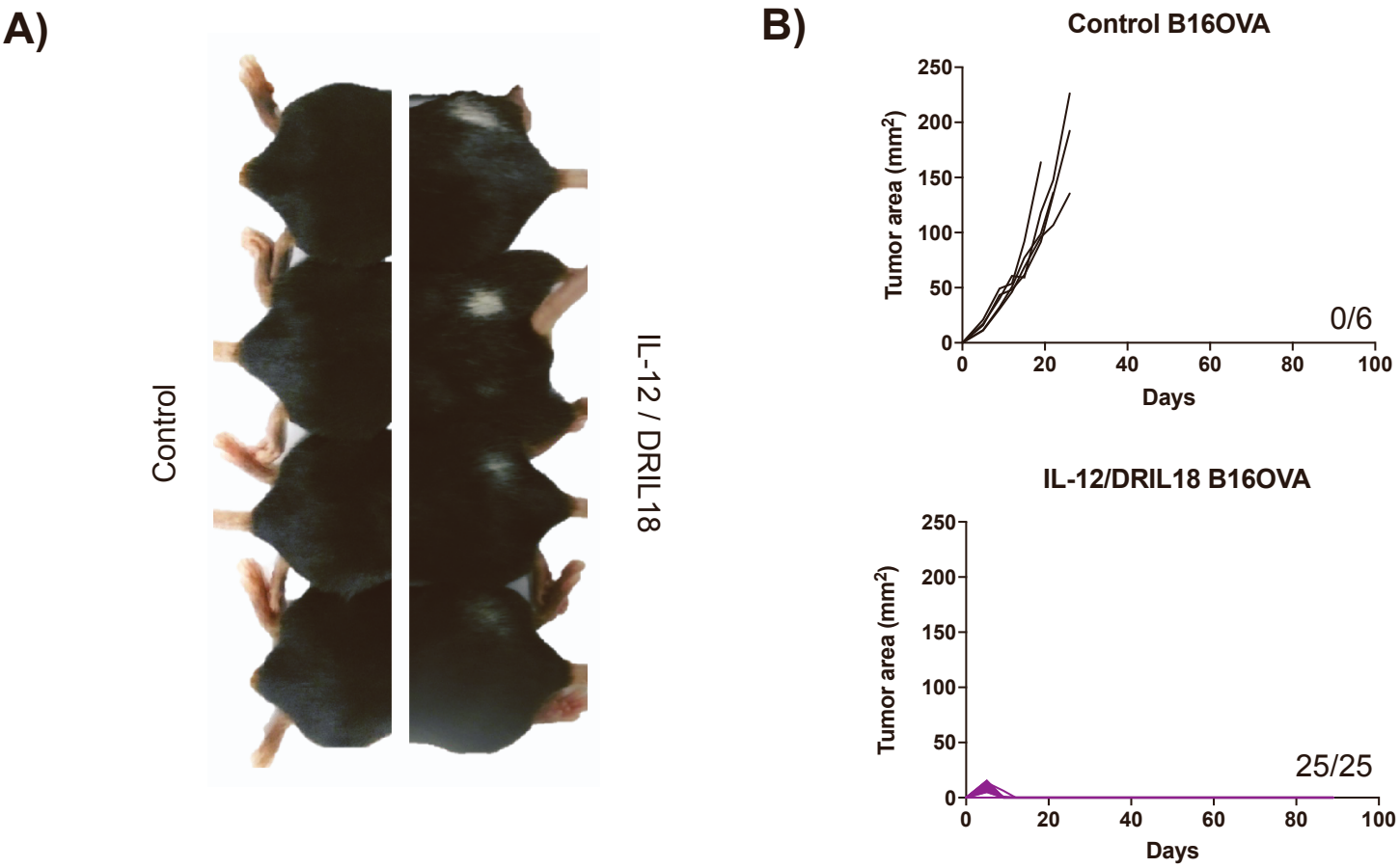

Figure S4. Vitiligo and long-term immunity in successfully treated mice. Related to Figure 1.
(A) Mice from experiments similar to those shown in Figures 1H and 1I showed de pigmentation (vitiligo) in the area of the fur where tumors had been injected and regressed. (B) Cured mice were kept at least 90 days following complete tumor regression after treatment with IL-12/DRIL18 mRNA electroporated Pmel-1 T cells and rejected a rechallenge with B16-OVA whilst a control group of naïve mice developed fast progressing lethal tumors. Experiments are representative of five similarly performed.

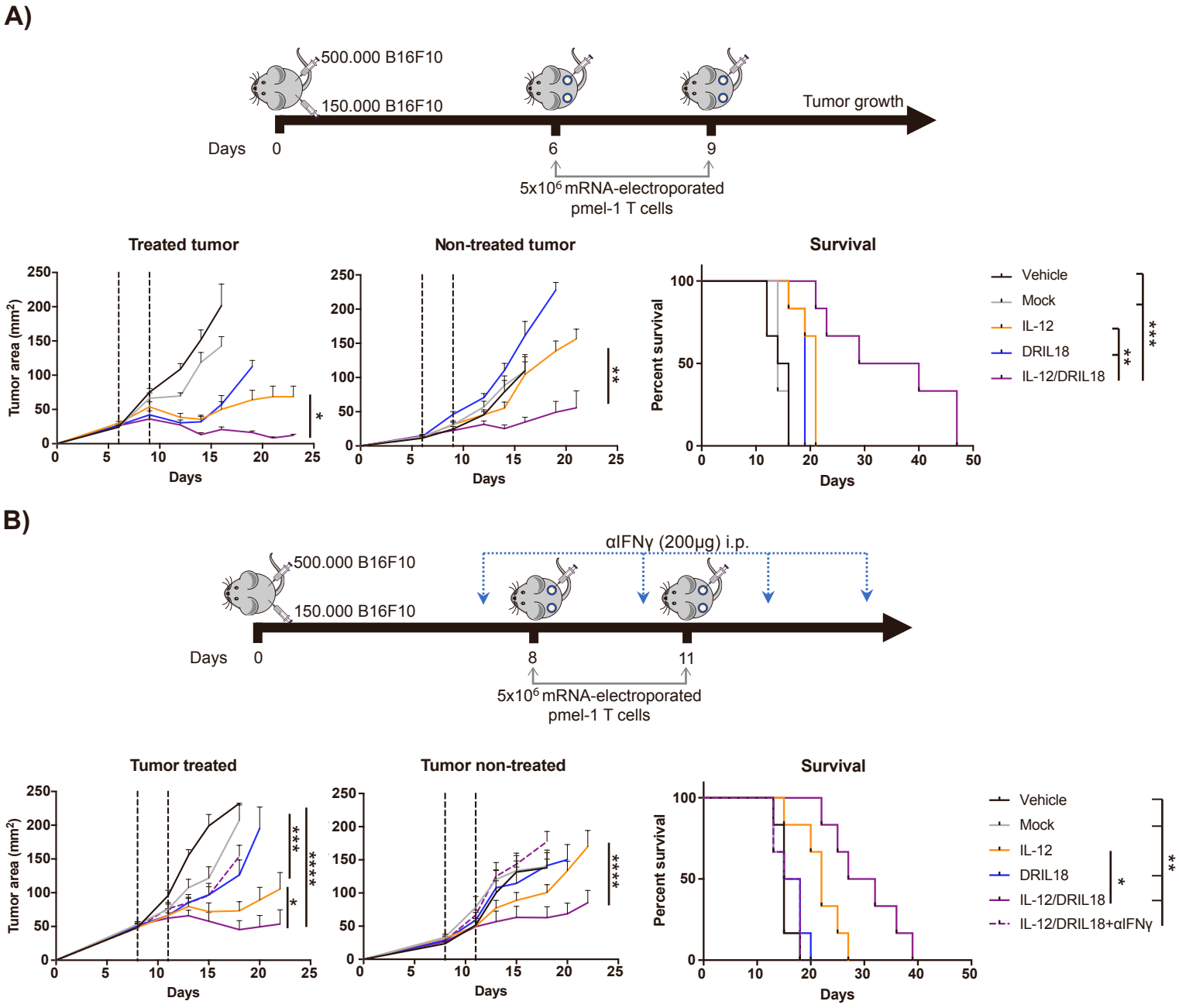

Figure S5. Efficacy of the scIL-12 and DRIL18 adoptive T cell strategy against B16F10 tumors. Related to Figure 1.
(A) Experiments as in Figure 1H were performed in mice bearing bilateral B16F10-derived tumors treated intratumorally on day +6 and +9 with mRNA-electroporated Pmel-1 cells or vehicle. Follow-up of tumor sizes of the indicated groups of treatment in the injected and non-injected tumor sites are shown. Overall survival of the mice in each group is also provided.
(B) Experiments as in A, but postponing the treatment onset to day +8 and giving to a group of mice treated with Pmel-1 (IL-12/DRIL18) a course of neutralizing anti-IFN-γ mAb.
Statistical comparisons were made with log-rank tests. Experiments are representative of at least two similarly performed. We randomly assigned 6 mice per group before tumor treatment. Data is represented as mean +/- SD.

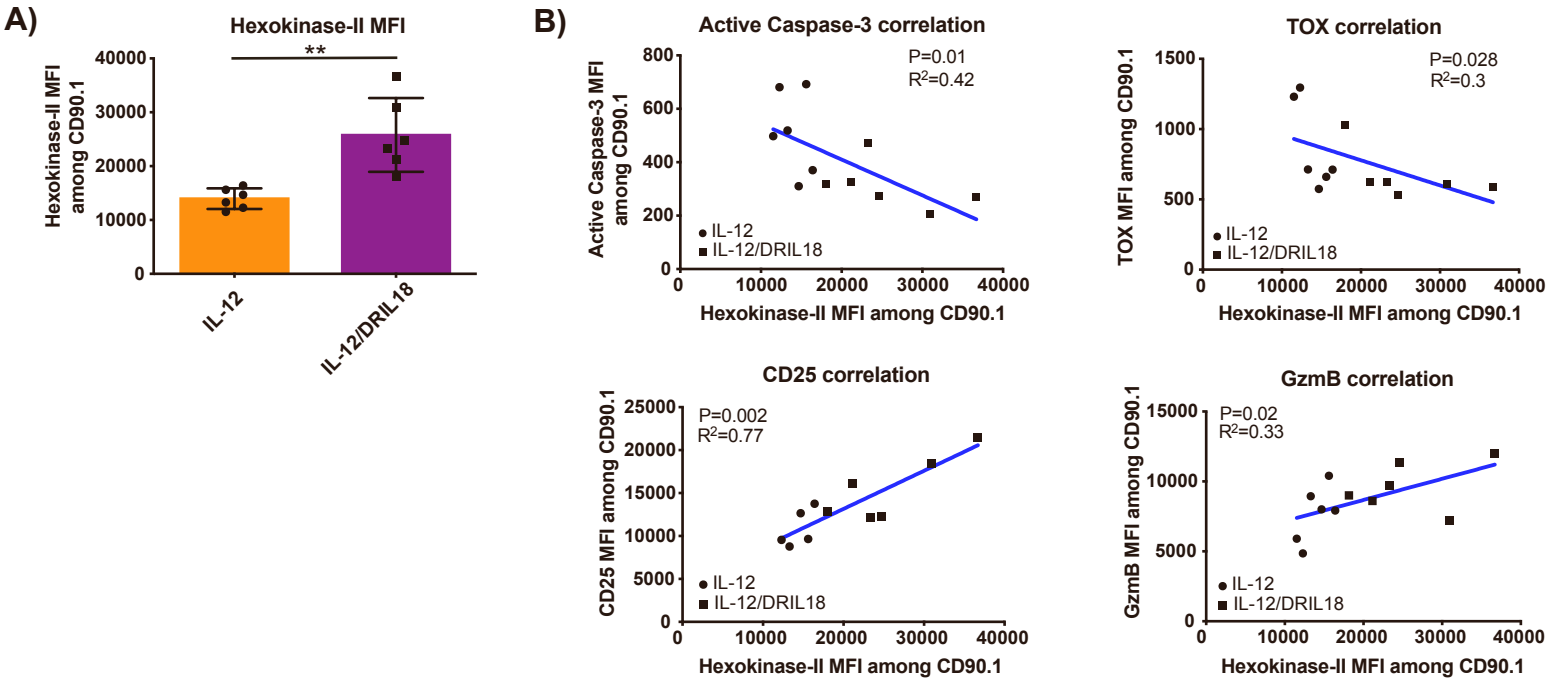

Figure S6. Hexokinase-II expression correlates with markers of functional T-cell activation. (A) Flow cytometry analysis of hexokinase -II expression in pmel-1 cells electroporated with the indicated mRNAs and recovered from B16OVA tumors 24h after being intratumorally injected. (B) Average intensity of expression of hexokinase-II in individual tumors compared with the average intensity of expression of the indicated markers (active caspase-3, CD25 surface expression, granzyme B intracellular expression and TOX expression). Regression statistics are shown in each graph. Statistical comparison in A was performed using one-way ANOVA test. Experiments are representative of two similarly performed. Related to Figure 4.

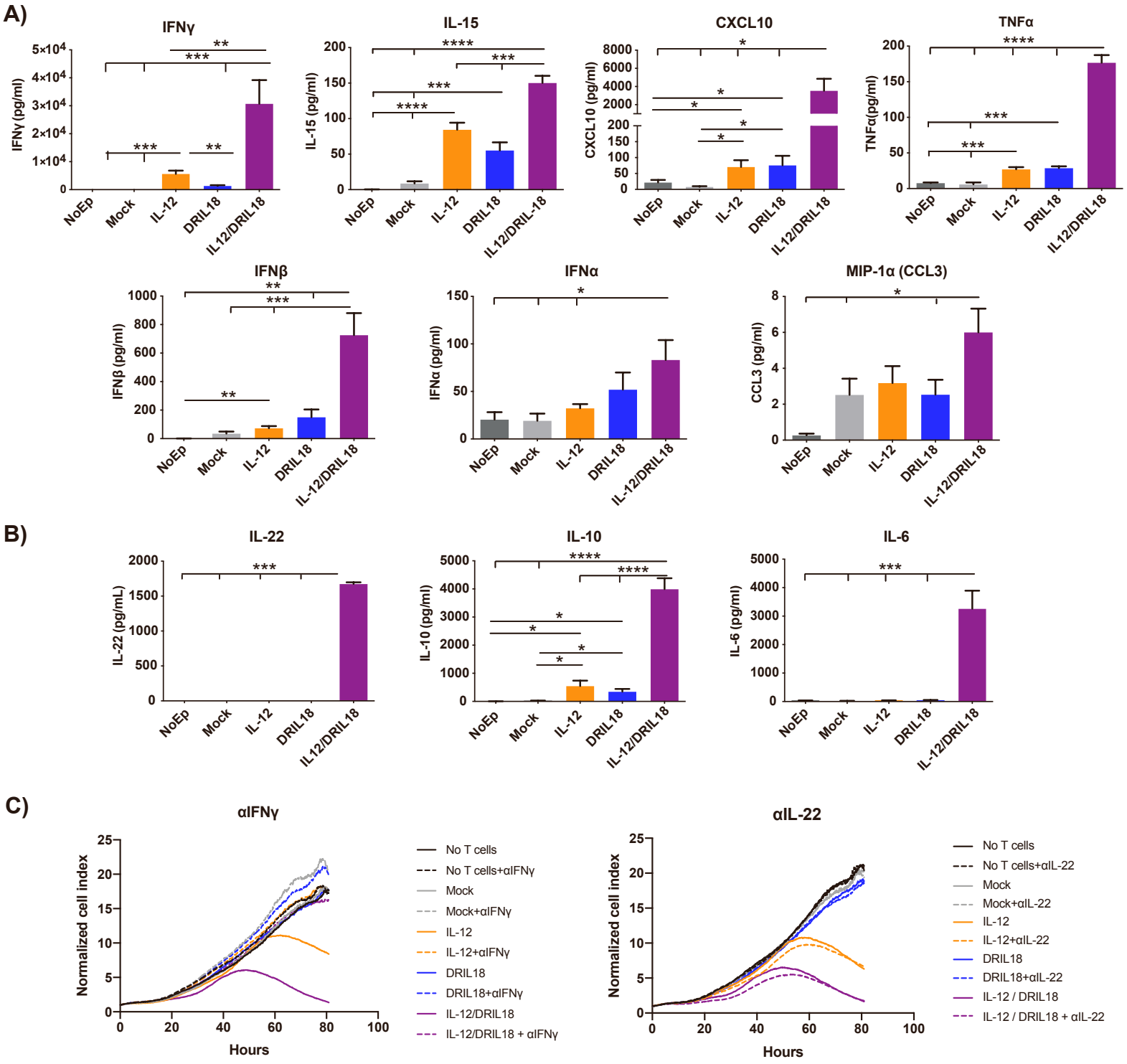

Figure S7. Electroporated DRIL18 and scIL-12 mRNA induce the production of endogenous cytokines. Related to Figure 5.
(A) Concentrations of the indicated immunostimulatory cytokines in 48h supernatants of Pmel-1 cells electroporated as indicated and assessed by a multiplex assay.
(B) Concentrations of potentially immunosuppressive cytokines in the same culture supernatants.
(C) Cytotoxicity experiments of the indicated mRNA-electroporated Pmel-1 cells against B16-OVA. Combinations of scIL-12/DRIL18 lymphocytes showed synergy. In the left graph neutralizing an anti-IFNγ mAb was added to some of the assays as well as a neutralizing anti-IL-22 mAb in some of the conditions shown in the right graph.
Experiments were repeated twice and statistical comparisons were performed with one-way ANOVA (A-B) or two-way ANOVA (C) tests. Biological duplicates were performed in all experiments. Data is represented as mean +/- SD.

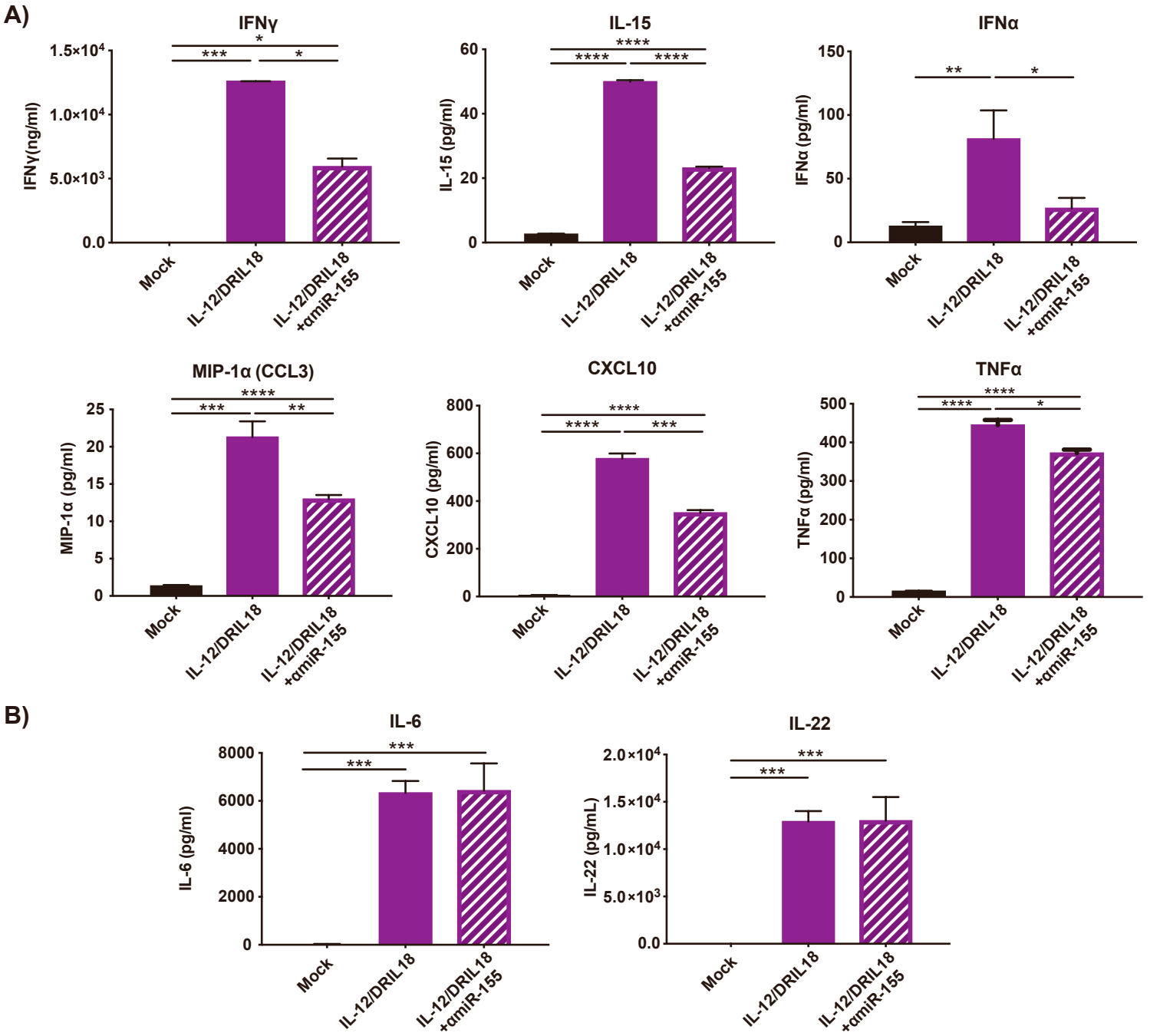

Figure S8. miR-155 degradation induced by coelectroporation of an antagomir reduces the production of T-cell stimulating cytokines. Related to Figure 5.

(A) Multiplex assessment of the concentrations of the indicated cytokines in the culture supernatants of pmel-1 cells electroporated with the indicated mRNAs with or without the antagomir.

(B) Experiments as in A testing the concentration of IL-6 and IL-12 that do not vary upon antagomir electroporation.

Statistical comparisons were performed using one-way ANOVA tests. Experiments are representative of two similarly performed. Biological duplicates were performed in all experiments. Data is represented as mean +/- SD.

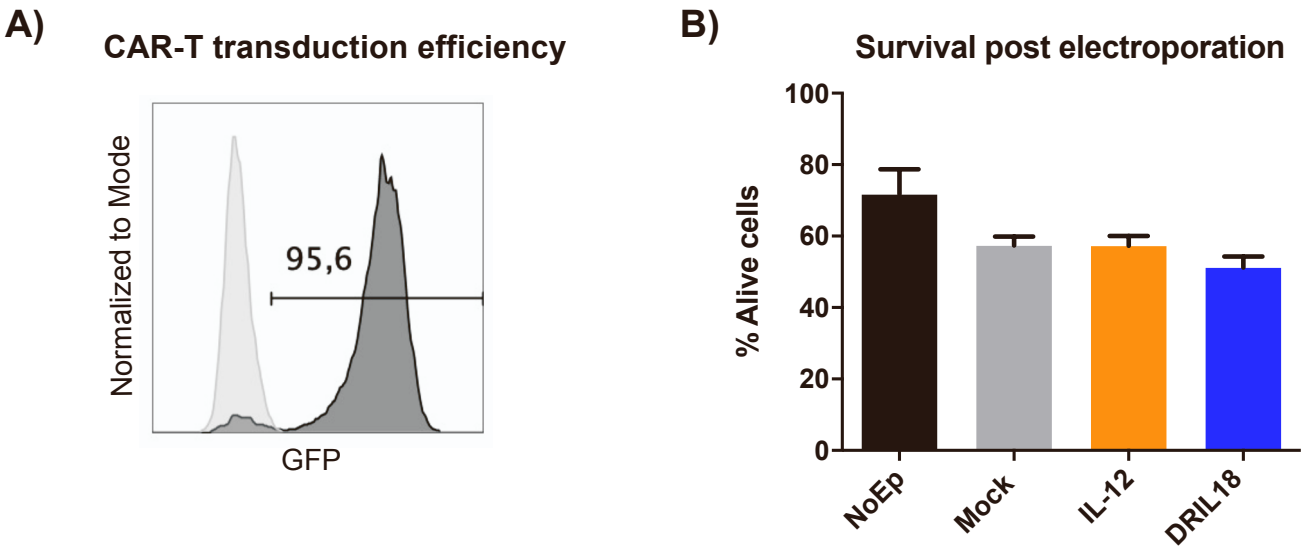

Figure S9. gp75 CAR transduction efficiency and viability following mRNA electroporation. Related to Figure 7.
(A) EGFP expression by CAR T cells transduced (black histogram) or untransduced T cell blasts (grey histogram) derived from splenocytes of C57Bl/6 mice by culture with plate-bound anti-CD3 mAb and soluble anti-CD28 mAb.
(B) Cell viability 6 h following electroporation procedures on CAR T cells.
Experiments are representative of at least two similarly performed. Biological duplicates were performed in all experiments. Data is represented as mean +/- SD.

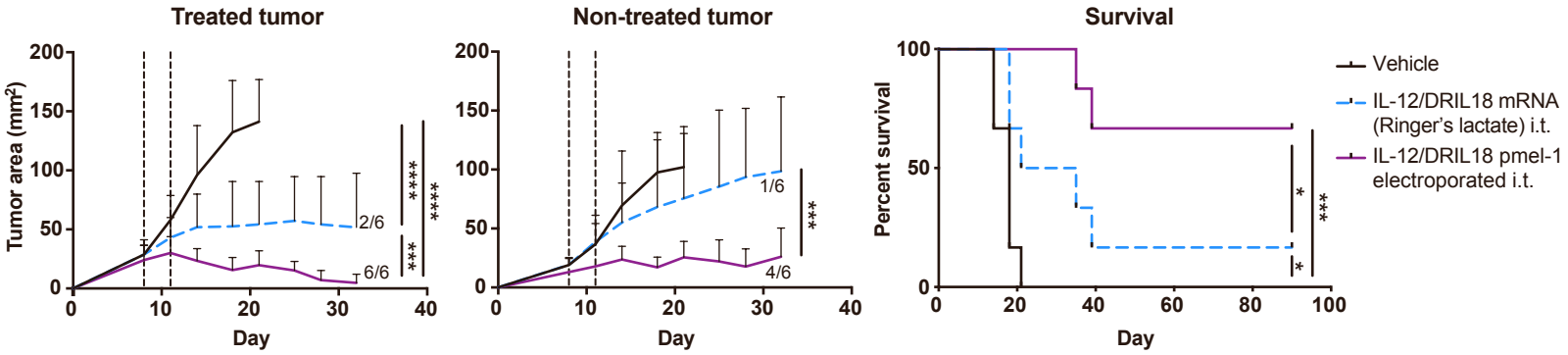

Figure S10. Comparison of naked mRNA enconding scIL-12 and DRIL18 given via intratumoral injection and intratumoral adoptive transfer of pmel-1 cells electroporated with the same mRNAs. Related to Figure 1.

Mice bearing bilateral B16OVA tumors were injected with scIL12 and DRIL18 encoding naked mRNA diluted in Ringer's lactate compared in its bilateral tumor effects with IL-12/DRIL18 electroporated pmel-1 cells given intratumorally. Both treatments were given on days +8 and +11. Black dotted lines represent the days of treatment. Tumor size follow-up of injected and contralateral tumors are provided with the overall survival achieved by the two different treatments. Tumor-free mice were also provided in each graph. Statistical comparisons were performed using two-way ANOVA test and log-rank tests for Kaplan-Meyer survival curves. Experiments are representative of two similarly performed.